Simultaneous estimation of earthquake source parameters and crustal Q value from broadband data of selected aftershocks of the 2001 M_w 7.7 Bhuj earthquake

A Saha, S Lijesh and P Mandal

National Geophysical Research Institute (Council of Scientific and Industrial Research), Hyderabad 500 606, Andhra Pradesh, India.
**Corresponding author. e-mail: prantik@ngri.res.in*

This paper presents the simultaneous estimation of source parameters and crustal Q values for small to moderate-size aftershocks (M_w 2.1–5.1) of the M_w 7.7 2001 Bhuj earthquake. The horizontal-component S-waves of 144 well located earthquakes (2001–2010) recorded at 3–10 broadband seismograph sites in the Kachchh Seismic Zone, Gujarat, India are analyzed, and their seismic corner frequencies, long-period spectral levels and crustal Q values are simultaneously estimated by inverting the horizontal component of the S-wave displacement spectrum using the Levenberg–Marquardt nonlinear inversion technique, wherein the inversion scheme is formulated based on the ω-square source spectral model. The static stress drops ($\Delta\sigma$) are then calculated from the corner frequency and seismic moment.

The estimated source parameters suggest that the seismic moment (M_0) and source radius (r) of aftershocks are varying from 1.12×10^{12} to 4.00×10^{16} N-m and 132.57 to 513.20 m, respectively. Whereas, estimated stress drops ($\Delta\sigma$) and multiplicative factor ($E_{\rm mo}$) values range from 0.01 to 20.0 MPa and 1.05 to 3.39, respectively. The corner frequencies are found to be ranging from 2.36 to 8.76 Hz. The crustal S-wave quality factor varies from 256 to 1882 with an average of 840 for the Kachchh region, which agrees well with the crustal Q value of the seismically active New Madrid region, USA. Our estimated stress drop values are quite large compared to the other similar size Indian intraplate earthquakes, which can be attributed to the presence of crustal mafic intrusives and aqueous fluids in the lower crust as revealed by the earlier tomographic study of the region.

1. Introduction

The 2001 Bhuj earthquake of M_w 7.7 is one of the largest intraplate earthquakes in recent time, which claimed a death toll of 20,000 people. This earthquake (lat. 23.412°N and long. 70.232°E) took place on 26th January 2001 along a south dipping reverse fault at 23 km depth in the Kachchh rift zone, which is situated in the northwestern corner of peninsular India (Mandal *et al.* 2004a, 2004b). The maximum intensity was reported to be X+ on MM scale (Rastogi *et al.* 2001). Within a span of 192 yrs (1819–2011), two large intraplate earthquakes, *viz.*, the 1819 Kachchh (M_w 7.8) and the 2001 Bhuj (M_w 7.7) have occurred in the Kachchh region. These earthquakes caused widespread destruction of properties and casualties (at least 22,000 people). In spite of such devastation, the earthquake hazard assessments for various seismogenic zones of India have grossly been undermined. Under these circumstances, it is proposed here to analyze the source parameters from the recorded aftershock

Keywords. Earthquake source parameters; crustal Q-value; simultaneous inversion; S-wave spectra; aftershocks.

data of Bhuj earthquake from Kachchh region of Gujarat province, India to properly assess the earthquake hazard of the region.

The 2001 Bhuj earthquake is perhaps one of the most enigmatic earthquake of the modern era as it raises some fundamental question regarding the existing paradigms for the earthquake, such as no surface expression of the causative fault, its occurrence in the stable continental regions away from the active plate boundaries and the high stress drop value associated with a smaller rupture area. This kind of intraplate earthquakes are rare and contributed 0.5% of the total annual global energy release through earthquakes (Johnston 1994). Only two intraplate regions in the world (e.g., Kachchh, India and New Madrid, USA) have got the unique distinction of experiencing large earthquakes of $M_w \geq 7.7$. But, the stress drop of the 2001 Bhuj mainshock was estimated to be around 200 bars (Antolik and Dreger 2003), which was larger than 1811–1812 New Madrid earthquakes with only 100 to 140 bars (Johnston and Schweig 1996). However, the 2001 Bhuj earthquake did not produce any clear discernible surface rupture except for a small 8 km-long zone of strike-slip faulting observed in the hanging wall of the causative fault plane (Wesnousky *et al.* 2001). The moment tensor inversion and aftershock studies delineate the causative fault for Bhuj earthquake, which is situated at 23 km of north of Kachchh Mainland Fault (KMF) and extends upto 40 km in depth with strike 65°, dip 50° and slip 50° that has been named as North Wagad Fault (Rastogi *et al.* 2001; Mandal *et al.* 2004a, 2004b). The rupture propagation study of the 2001 Bhuj mainshock using the waveform inversion revealed that the mainshock did release ∼ 65% of moment energy with a peak slip of 12.4 m at the deeper part of fault (10–35 km), whereas, the remaining moment energy was released at the sallower part (0–10 km) with a maximum slip of 6.5 m[4]. Singh *et al.* (2004) proposed that the rupture process was quite slow and radially symmetric for the 2001 Bhuj earthquake.

Numerous attempts have been made to estimate the static stress drop for the 2001 Bhuj mainshock using the locations of aftershocks (Negishi *et al.* 2001; Bodin and Horton 2004; Singh *et al.* 2004). Negishi *et al.* (2001) obtained a static stress drop ranging from 12.6 to 24.6 MPa, for an equivalent source radius varying from 20 to 25 km. But, Bodin and Horton (2004) calculated a static stress drop of 16.0 ± 2 MPa over a rupture area of 1300 km^2. Singh *et al.* (2004) suggest that a frictional sliding model with an average dynamic stress drop of about 12 MPa and the ratio of rupture to shear wave velocity of 0.7 could satisfactorily explain the source complexity observed for the 2001 Bhuj mainshock. Based on waveform modelling, Antolik and Dreger (2003) proposed a stress drop value of 20.7 MPa with a small fault length of 45 km for the 2001 Bhuj mainshock. Mandal and Johnston (2006) found that the stress drop values show scatter above $10^{14.5}$ N-m for Bhuj aftershocks. The continued aftershock activity for more than 10 years, further, demonstrates the source complexity involved in generating these deeper earthquakes. Thus, this large variation in estimated source parameters of Bhuj mainshock suggests that the study of source parameters of its aftershocks became an important issue because of their continued nature as well as deeper origin (focal depths ∼10–40 km).

In this study, we use a two-stage methodology for estimating the source parameters, which is mentioned below:

1. Spectral analysis of S-wave using SEISAN software (Havskov and Ottemoller 2003).
2. Inversion modelling using Levenberg–Marquadt non-linear inversion technique.

We apply the above technique to the broadband data of 136 well located aftershocks of the 2001 Bhuj earthquake, to estimate their source parameters and crustal Q values. Finally, the estimated parameters are used to understand the seismogenesis of the 2001 Bhuj earthquake sequence.

2. Geology and tectonics of the Kachchh region

Geologically, Quaternary/Tertiary sediments, Deccan volcanic rocks and Jurassic sandstones resting on Archean basement mainly characterize the Kachchh region (Gupta *et al.* 2001). The sediment fill thickens from less than 500 m in the north to over 4000 m in the south and from 200 m in the east to over 2500 m in the west (Gupta *et al.* 2001). To the north, Precambrian basement rocks are exposed in Meruda Takkar and Nagar Parkar (in Pakistan) hills (Biswas 1987). The Mesozoic rift-related extensional structures of the Kachchh basin got reactivated as strike-slip or reverse faults as a result of regional compressive stresses due to collision of Indian and Eurasian plates since Neogene times (Biswas 1987). The focal mechanisms of some earthquakes indicate reverse faulting suggesting ongoing inversion tectonics in the Kachchh basin (Chung and Gao 1995).

Major structural features of the Kachchh region include several E–W trending faults/folds as shown in figure 1. The rift zone is bounded by a north dipping Nagar Parkar Fault in the north and a south dipping Kathiawar Fault in the south. Other major faults in the region are the E–W trending Allah Bund Fault, Island Belt Fault, Kachchh Mainland

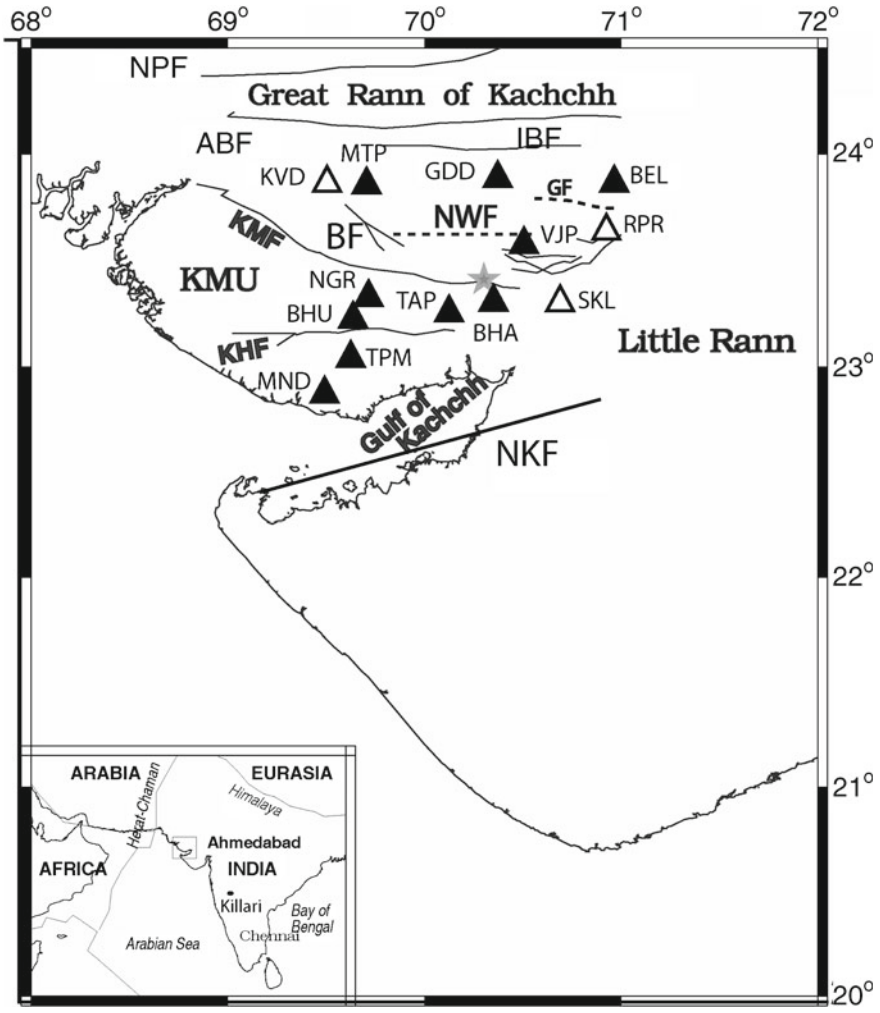

Figure 1. Location of the 10 mobile broadband stations (marked by solid black triangles), which were deployed during 2006–2010, alongwith the 2001 Bhuj mainshock epicenter (grey star symbol) while three stations, which were deployed in 2001, are shown by open triangles. Stations: VJP: Vajepar, TAP: Tapar, MTP: Motapaya, GDD: Gadhada, BHA: Bhachau, BEL: Bela, NGR: Nagor, BHU: Bhuj, TPM: Tappar (Mundra), MND: Mandvi, KVD: Kavada, RPR: Rapar, SKL: Samkhiyali. KMU: Kachchh mainland uplift. Major faults (solid lines): ABF, Allah Bund Fault; IBF, Island belt fault; KMF, Kachchh mainland fault; KHF, Katrol hill fault; NPF, Nagar Parkar fault; NKF, North Kathiawar fault; BF, Banni fault. And, NWF (North Wagad fault), the causative fault for 2001 Bhuj earthquake and Gedi fault, are shown by dotted line. The inset is showing the key map for the area, where, the study area is shown by a grey square. The epicentral location of the 1993 Latur earthquake is also shown by a grey dot.

Fault and Katrol Hill Fault. In addition, several NE and NW trending small faults/lineaments are observed (Biswas 1987). Seismic, gravity and magneto-telluric surveys indicate undulated basement with 2–5 km deep sediments and Moho depth at 35–43 km in southern Kachchh region (Gupta *et al.* 2001; Reddy *et al.* 2001). Prior crustal velocity investigations in Kachchh region suggest a large variation in the estimated Moho depths that varies from 37 to 48 km (Kumar *et al.* 2001; Reddy *et al.* 2001; Mandal 2006). Recently, a P-receiver function study also delineates a 4–6 km crustal as well as 6–12 km asthenosphereic thinning beneath the Kachchh rift zone (Mandal 2011). The crustal and lithospheric thicknesses obtained by Mandal (2011) vary from 35–43 and 62–90 km, respectively. In general, this region is very complex as it contains faults of multiple orientations and different natures (Biswas 1987). Focal mechanism solutions of a few of the major aftershocks obtained from waveform inversion of broadband data indicate a dominant reverse movement on the NWF (Mandal and Horton 2007). The focal mechanism solutions of 444 aftershocks (using 8–12 first motions) suggest that the focal mechanisms ranged between pure reverse and pure strike slip except some pure dip slip solutions (Mandal and Horton 2007). These mechanisms also suggest that the reverse movements on a preferred south-dipping plane mainly characterize the NWF, whereas, the strike slip movement along an almost vertical plane dominates the Gedi Fault (GF) (Mandal *et al.* 2009).

3. Past seismicity

The Kachchh region lies in the highest seismicity zone V, which is potential for M8 magnitude (BIS 2002). Large earthquakes have been occurring in the Kachchh region since historical times. It has been inferred, based on the radiocarbon dating that an earthquake occurred between 885 and 1035 AD along the Allah Bund Fault (Rajendran and Rajendran 2001). From historical records of earthquakes, a large earthquake occurred in 1030 AD (Williams 1958). In 1668, a moderate earthquake occurred west of Kachchh, with an epicenter at 24°N, 68°E (Rajendran and Rajendran 2001). The largest earthquake in the region occurred on June 6, 1819. This M_w 7.8 earthquake resulted in a 90 km long, 6.3 km wide and 4.3 m high ridge and created what is known as the Allah Bund (Johnston and Schweig 1996; Rajendran and Rajendran 2001). Between 1821 and 1996, 16 moderate earthquakes of magnitude varying from 4.2 to 6.1 have occurred in the region (Rajendran and Rajendran 2001). The last damaging earthquake of M_w 6.0 (Intensity IX) prior to the most recent M_w 7.7 2001 Bhuj event occurred along the Katrol Hill Fault near Anjar, Gujarat in 1956, which claimed 115 lives (Chung and Gao 1995). This earthquake was apparently a shallow reverse rupture, but did not rupture the surface. Most recently there was an earthquake in 1992 (Dodge *et al.* 1996), which was 19 ± 4 km deep. On December 24, 2001, an M5 earthquake struck north of Bhuj, the teleseismically-determined epicenter close to the western end of the Island Belt fault (Bodin and Horton 2004). The devastating 2001 Bhuj earthquake occurred on the ENE–WSW trending and south dipping reverse fault at a depth of 23 km (figure 1).

4. Aftershock data

In this study, we use 384 good seismograms (high S/N ratio) of 144 Bhuj aftershocks recorded at 3–5 digital seismograph stations. These aftershocks of moment magnitude 2.1 to 5.1 were recorded by the close digital Kachchh seismological network of National Geophysical Research Institute (NGRI), Hyderabad during February 2001 to March 2010. The network consists of 13 3-component broadband seismographs (figure 1). Each seismograph is equipped with a 24-bit Reftek recorder (with an external hard disk of 2 GB and GPS timing system) and 3-component broadband sensors (CMG3T and CMG40T). During this period, the broadband stations were situated between latitude 23.24^0–23.87^0N and longitude 69.72^0–70.37^0E. All broadband stations are installed on the hard sediment resulting in good signal-to-noise ratio. The P- and S-arrival times recorded from the network enabled us to obtain a better estimation of hypocentral parameters (error in epicentral location <2 km, focal depth estimation <6 km and rms of P-residual <0.3 s). A strong Sp converted phase appearing 0.7–1.1 s prior to the S-arrival, which is generated from the sedimentary-basement transition, characterizes the seismograms for Bhuj aftershocks (Mandal 2007). To avoid the influence of Sp converted phase on the event location, we picked strong S-phase on the horizontal components of seismograms leaving the weak beginning of the S wave train.

Table 1. *One-dimensional P-wave velocity, S-wave velocity and density model (Berteusen 1977; Mandal 2007).*

Depth (km)	V_p (km/s)	V_s (km/s)	ρ (kg/m^3)
0.0 – 2.0	2.92	1.69	1700
2.0 – 10.0	5.93	3.43	2670
10.0 – 16.0	6.18	3.57	2750
16.0 – 29.0	6.40	3.70	2820
29.0 – 40.0	6.97	4.03	3000
40.0 – 100.0	8.20	4.74	3390

5. Location, delineation and characterization of the causative fault

Aftershock locations are obtained using the program HYPO71Pc (Lee and Valdes 1985) and the modified average one-dimensional crustal velocity model (Mandal 2007; table 1). The velocity model consists of six layers, the tops of which are at 0.0, 2.0, 10.0, 16.0, 29.0, and 40.0 km, with P-wave velocities of 2.92, 5.93, 6.18, 6.40, 6.97, and 8.20 km/s, respectively (Mandal 2007). The distance between station and epicenters varies from 5 to 90 km. This network provides an azimuthal gap of less than 180°. The average location rms was 0.03 s. The mean horizontal and vertical single 68% confidence estimates are 2.0 and 6.0 km, respectively, for the aftershocks (table 2).

The estimated relatively accurate hypocentral parameters (error in epicentral location <1.5 km, focal depth estimates <3 km and rms of P-residual <0.3 s) of 144 selected aftershocks (2001–2010) of the 2001 Bhuj mainshock show that most of the events are mainly clustered within an E–W trending crustal volume below the main rupture zone of the 2001 Bhuj mainshock, which extends 55 km in N–S (latitude 23.25°–23.75°N), 45 km in E–W (longitude 70.0°–70.55°E) and 35 km in depth (from 1 to 36 km) (figure 2a–c). However, a few events are clustered along the GF while some scattered events are also located along the ABF and IBF

Table 2. *Estimated hypocentral parameters for selected 144 Bhuj aftershocks.*

Ev. nos	YearMnDa	Ori. time (HrMnSs)	Lat. (°)	Long. (°)	Depth (km)	M_w
No 1	2001 208	1029 54.0	23.341	70.399	21.9	4.1
No 2	2001 208	0324 56.0	23.260	70.320	17.0	4.1
No 3	2001 208	0931 52.0	23.430	70.499	26.3	4.4
No 4	2001 208	1411 55.0	23.389	70.279	29.2	3.3
No 5	2001 208	1653 52.0	23.710	70.444	28.0	4.4
No 6	2001 208	1704 51.0	23.320	70.330	20.9	3.5
No 7	2006 406	1202 52.9	23.780	70.740	3.1	4.8
No 8	2006 406	1759 18.2	23.340	70.390	29.3	5.1
No 9	2009 411	1231 46.1	23.491	70.267	15.5	2.8
No 10	2009 412	1842 10.8	23.420	70.148	17.8	3.3
No 11	2009 414	1219 16.7	23.387	70.344	10.0	2.6
No 12	2009 414	1943 20.0	23.472	70.290	17.5	2.1
No 13	2009 415	0913 49.5	23.401	70.188	33.4	3.1
No 14	2009 415	1420 34.3	23.294	70.258	14.6	2.7
No 15	2009 415	2115 14.6	23.578	70.505	14.9	3.1
No 16	2009 416	0018 55.5	23.434	70.185	12.4	3.4
No 17	2009 416	1806 41.8	23.554	70.343	9.8	2.4
No 18	2009 419	1941 56.4	23.544	70.307	15.9	2.7
No 19	2009 419	1950 27.6	23.564	70.443	22.5	2.5
No 20	2009 422	1543 17.3	23.470	70.397	24.0	2.6
No 21	2009 422	2253 29.9	23.434	70.368	17.8	2.2
No 22	2009 423	0540 44.9	23.392	70.329	22.5	2.1
No 23	2009 423	2042 52.2	23.361	70.390	22.4	2.9
No 24	2009 425	0347 23.3	23.475	70.405	26.2	2.2
No 25	2009 425	0424 28.0	23.382	70.352	24.7	2.5
No 26	2009 425	1046 33.3	23.476	70.153	15.9	2.7
No 27	2009 425	1526 28.9	23.450	70.174	0.7	2.4
No 28	2009 425	1816 21.5	23.449	70.445	15.5	2.4
No 29	2009 425	1900 50.4	23.466	70.179	20.1	2.5
No 30	2009 426	1403 26.4	23.458	70.415	20.3	2.2
No 31	2009 427	0752 17.9	23.373	70.383	20.2	2.3
No 32	2009 428	1914 36.2	23.324	70.259	13.9	2.3
No 33	2009 429	1525 9.3	23.381	70.236	35.5	2.5
No 34	2009 429	2254 11.5	23.534	70.433	19.6	2.3
No 35	2009 5 2	1602 0.6	23.546	70.430	24.3	2.4
No 36	2009 5 3	2103 30.1	23.461	70.109	28.8	2.7
No 37	2009 5 4	0532 49.9	23.614	69.977	24.4	2.2
No 38	2009 6 3	2231 16.3	23.375	70.082	20.5	2.6
No 39	2009 6 5	0418 1.8	23.578	70.428	22.6	2.6
No 40	2009 6 5	1135 14.5	23.428	70.245	24.9	2.4
No 41	2009 6 6	1027 32.1	23.543	70.233	10.0	2.4
No 42	2009 6 7	0833 39.8	23.423	70.357	28.9	3.1
No 43	2009 6 7	1125 51.2	23.429	70.368	28.0	3.0
No 44	2009 6 9	0403 31.9	23.537	70.057	22.4	2.6
No 45	2009 6 9	1119 22.5	23.452	70.335	24.0	2.3
No 46	2009 6 9	2359 46.3	23.536	70.032	10.9	2.4
No 47	2009 610	1414 24.2	23.463	70.349	15.7	2.3
No 48	2009 610	1541 26.2	23.587	70.491	15.7	2.7
No 49	2009 611	2151 21.8	23.548	70.049	14.2	2.6
No 50	2009 612	0043 58.7	23.371	70.149	24.0	2.3
No 51	2009 614	0534 38.1	23.419	70.133	18.0	2.4
No 52	2009 621	0359 47.9	23.432	70.180	24.5	2.5
No 53	2009 621	1856 14.5	23.496	70.365	18.0	2.3
No 54	2009 622	0811 34.3	23.496	70.433	21.9	2.5

Table 2. *(Continued)*

Ev. nos	YearMnDa	Ori. time (HrMnSs)	Lat. (°)	Long. (°)	Depth (km)	M_w
No 55	2009 623	1943 8.3	23.482	70.280	17.0	2.7
No 56	2009 623	2059 25.1	23.514	70.027	17.7	2.3
No 57	2009 624	0119 29.1	23.505	70.201	18.3	2.3
No 58	2009 624	0236 45.4	23.758	70.462	16.6	2.7
No 59	2009 624	0944 58.6	23.405	70.132	18.6	3.2
No 60	2009 624	1538 42.1	23.388	70.308	8.6	2.9
No 61	2009 625	0807 51.9	23.489	70.397	21.5	3.2
No 62	2009 627	0156 37.7	23.495	70.394	9.5	3.3
No 63	2009 627	0201 12.8	23.489	70.394	14.7	3.0
No 64	2009 627	1345 36.0	23.497	70.188	15.3	2.7
No 65	2009 627	1737 55.2	23.381	70.202	29.1	3.2
No 66	2009 628	0603 40.5	23.469	70.225	15.4	2.8
No 67	2009 628	0832 12.0	23.402	70.350	21.1	3.3
No 68	2009 629	0030 27.4	23.477	70.169	16.0	2.7
No 69	2009 630	0054 8.9	23.510	70.409	15.8	2.5
No 70	2009 630	1206 44.5	23.490	70.330	14.4	2.5
No 71	2009 630	1252 23.2	23.506	70.085	16.1	2.8
No 72	2009 7 1	2234 55.2	23.431	70.110	15.4	2.6
No 73	2009 7 5	1915 8.9	23.473	70.241	19.6	2.7
No 74	2009 7 8	0621 12.1	23.572	70.158	15.6	3.1
No 75	2009 7 8	1128 3.4	23.640	70.221	16.1	2.3
No 76	2009 710	1239 19.5	23.433	71.170	29.2	2.8
No 77	2009 711	2222 18.2	23.444	70.431	21.3	2.5
No 78	2009 713	0040 5.8	23.391	70.319	12.0	2.7
No 79	2009 713	0535 28.3	23.391	70.314	10.2	2.6
No 80	2009 717	0924 57.3	23.677	70.424	29.9	2.8
No 81	2009 719	1055 34.6	23.680	70.520	15.2	2.3
No 82	2009 720	1947 1.0	23.517	70.344	13.3	2.6
No 83	2009 721	1931 49.8	23.490	70.228	17.8	2.6
No 84	2009 723	0713 4.3	23.465	70.492	15.4	2.5
No 85	2009 723	1721 51.9	23.587	70.095	16.0	3.3
No 86	2009 724	1230 17.3	23.446	70.344	24.9	2.3
No 87	2009 725	1225 0.9	23.513	70.303	13.8	2.4
No 88	2009 727	1722 1.4	23.490	70.057	25.9	2.2
No 89	2009 728	0207 11.3	23.451	70.388	19.7	2.5
No 90	2009 728	2318 16.4	23.812	70.677	9.8	2.3
No 91	2009 8 1	1615 27.1	23.482	70.196	21.2	2.2
No 92	2009 8 1	1953 17.3	23.813	70.681	9.6	2.2
No 93	2009 8 2	1852 35.8	23.491	70.092	23.3	2.5
No 94	2009 8 3	1452 24.1	23.474	70.261	15.6	2.3
No 95	2009 8 3	1751 28.6	24.315	69.811	14.4	3.2
No 96	2009 8 5	0418 29.5	23.491	70.383	23.0	2.4
No 97	2009 8 6	0204 41.4	23.453	70.158	14.9	2.5
No 98	2009 8 7	0415 53.1	23.466	70.382	25.3	2.3
No 99	2009 8 8	0201 36.8	23.401	70.347	23.6	3.1
No 100	2009 811	0554 22.8	23.741	70.470	12.0	2.4
No 101	2009 811	0631 44.5	23.521	70.195	8.9	2.3
No 102	2009 816	1013 52.7	23.550	70.295	18.0	2.5
No 103	2009 817	1728 6.6	23.543	70.442	20.3	2.4
No 104	2010 131	1243 58.8	23.423	70.211	23.8	2.6
No 105	2010 2 2	1511 55.7	23.581	70.376	25.9	2.4
No 106	2010 2 4	0447 49.8	24.101	69.882	15.7	2.8
No 107	2010 2 4	0512 2.9	23.413	70.256	26.4	2.6
No 108	2010 2 5	1514 37.6	23.505	70.247	16.1	3.1

Table 2. *(Continued)*

Ev. nos	YearMnDa	Ori. time (HrMnSs)	Lat. (°)	Long. (°)	Depth (km)	M_w
No 109	2010 2 7	1244 28.0	23.496	70.475	22.2	3.3
No 110	2010 2 7	2240 16.0	23.488	70.420	20.4	2.3
No 111	2010 2 8	0954 49.9	23.504	70.493	20.7	2.1
No 112	2010 211	0906 56.7	23.474	70.136	24.4	2.1
No 113	2010 211	1713 1.8	23.352	70.399	21.5	2.2
No 114	2010 211	1719 29.5	23.488	70.113	20.5	2.6
No 115	2010 212	1422 31.3	23.544	70.265	13.3	2.8
No 116	2010 212	1532 18.6	23.427	70.188	31.3	2.4
No 117	2010 212	2132 13.7	24.711	70.712	21.2	2.8
No 118	2010 213	0005 43.9	23.538	70.205	16.0	2.1
No 119	2010 215	0054 44.5	23.548	70.373	16.6	3.3
No 120	2010 215	0329 42.8	23.539	70.077	0.9	2.2
No 121	2010 215	1626 20.6	23.464	70.334	27.6	2.0
No 122	2010 218	1255 54.8	23.397	70.322	19.0	2.2
No 123	2010 219	0900 0.7	23.397	70.330	33.6	2.2
No 124	2010 219	2101 39.7	23.471	70.161	23.6	2.2
No 125	2010 220	0726 6.7	23.416	70.443	19.6	2.2
No 126	2010 221	0238 49.3	23.479	70.428	17.7	2.6
No 127	2010 224	1405 52.1	23.579	70.256	9.9	2.1
No 128	2010 224	1838 6.9	23.348	70.540	16.7	2.3
No 129	2010 225	0604 25.3	23.404	70.418	21.1	2.7
No 130	2010 225	1011 36.6	23.388	70.231	9.9	2.6
No 131	2010 225	1428 16.5	23.400	70.365	21.0	3.2
No 132	2010 3 1	0925 18.9	23.248	70.228	14.0	3.4
No 133	2010 3 6	1748 29.8	23.392	70.307	32.1	2.4
No 134	2010 310	0344 3.7	23.391	70.365	21.6	2.6
No 135	2010 310	1514 17.0	23.432	70.254	26.0	2.4
No 136	2010 310	1638 22.7	23.602	70.062	15.0	2.6
No 137	2010 310	2001 46.5	23.471	70.193	18.9	2.4
No 138	2010 311	0034 49.2	23.599	70.408	25.3	2.5
No 139	2010 4 2	1831 33.6	23.519	70.315	18.6	2.2
No 140	2010 4 6	1256 41.9	23.398	70.340	23.8	2.6
No 141	2010 4 8	1517 50.3	23.322	70.198	30.8	2.4
No 142	2010 4 8	1654 54.0	23.589	70.526	9.1	2.2
No 143	2010 411	1758 39.9	23.521	70.403	16.5	2.3
No 144	2010 411	2258 47.2	23.477	70.183	19.5	2.3

(figure 2a). The N-S hypocentral depth distribution of aftershocks suggests a marked concentration along the south dipping NWF (figure 2b). The upward projection of this south-dipping plane (i.e., NWF, North Wagad Fault) touches the ground surface at Burudia village (∼23.6°N) and extending along Wagad uplift (figure 2c). This result is in good agreement with the geological trenching data of McCaplin and Thakkar (2001). The strike of the aftershock zone agrees well with the south-dipping E–W striking nodal plane of the mainshock (Mandal and Horton 2007). However, the E–W cross section shows a marked change (∼10–15 km) in seismogenic depth across the main rupture zone of the 2001 Bhuj mainshock (figure 2c). This change in seismogenic change could be attributed to the lateral variation in maficness across the main rupture zone (Mandal and Pandey 2010).

6. Methodology for estimating earthquake source parameters

First, we compute the S-spectra using the in-built program of SEISAN software (Havskov and Ottemoller 2003), where no-correction for the Q is applied. Next, these spectra are used as input data for the Fletcher's simultaneous inversion technique for estimating earthquake source parameters and crustal Q values (Fletcher 1995). However, here we used the Lavenberg–Marquart

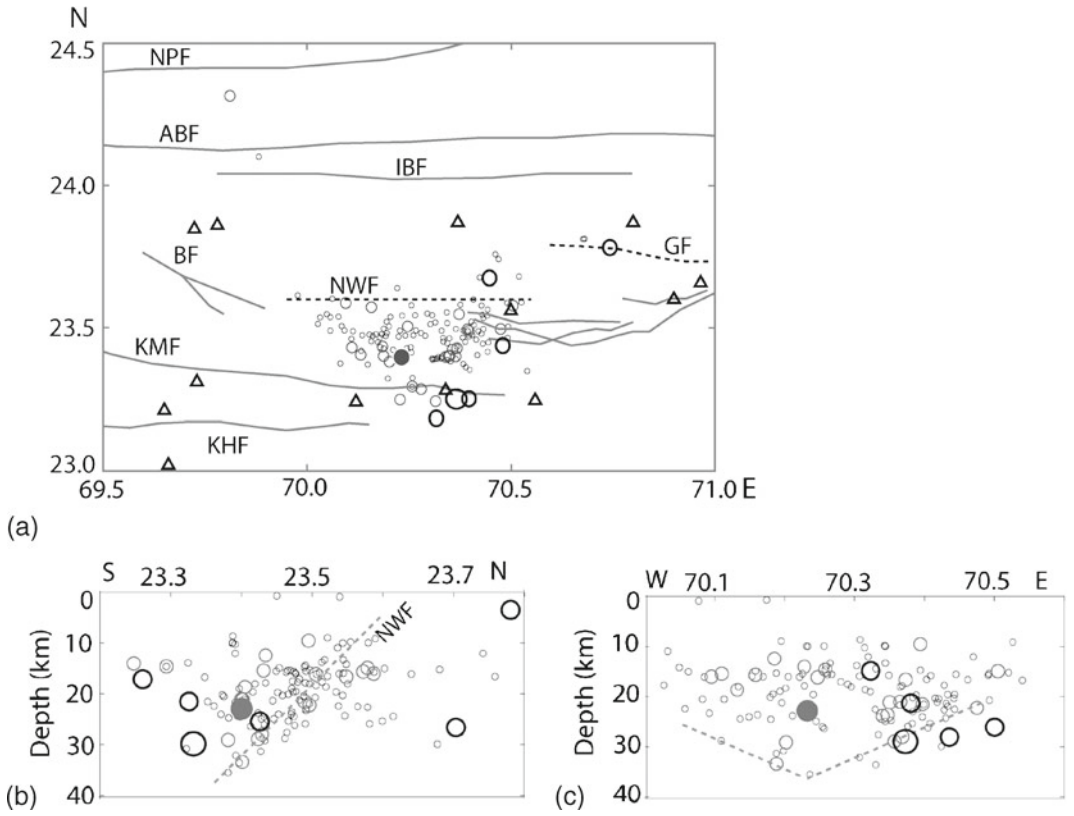

Figure 2. (**a**) Epicenteral locations of the 136 selected aftershocks (M_w 2.1–3.4), which have occurred in the Kachchh seismic zone during March 2009 to March 2010, are shown by grey open circles. Epicentral locations of six selected 2001 aftershocks (M_w 3.3–4.4) and two selected 2006 aftershocks (M_w 4.8–5.1) are also shown. And, small grey open circles mark aftershocks with M_w 1.1–2.9 while medium grey open circles mark the epicenters of aftershocks with M_w 3–3.9. And, medium black open circles are showing the epicenters of aftershocks with M_w 4.0–4.8. The inferred causative faults are shown by grey dotted lines and are marked as NWF (North Wagad Fault) and GF (Gedi fault), respectively. The solid large grey circle shows the epicenter of the 2001 Bhuj mainshock of M_w 7.7 while large open black circle shows the event having highest magnitude ($\sim M_w$ 5.1) in this study. (**b**) Hypocentral depth plots of selected 144 earthquakes in E–W direction. And, the dotted grey line marks the causative NWF. (**c**) Hypocentral depth plots of the selected earthquakes in N–S direction. Grey dotted lines mark the change in seismogenic depth.

inversion method instead of singular value decomposition technique as used by Fletcher (1995). This two-stage technique is discussed below:

6.1 *Two-stage technique to estimate earthquake source parameters and crustal Q values*

In the first stage, we estimate the displacement S-wave spectra from the horizontal components of the three-component digital recording, using spectral technique in-built in the SEISAN software (Havskov and Ottemoller 2003). After obtaining the required spectra with low noise level (S/N ratio is high enough), we use it as the input data for the Levenberg–Marquadt inversion modelling. The Levenberg–Marquadt algorithm combines beneficial aspects of gauss Newton and steepest descend methods, which facilitates the faster convergence of the solution. First, we select the initial guessed values for corner frequency and long period spectral level from the respective spectra. Next, we use these initial values to calculate the inverted spectra using the ω-square source spectral model. Then, a normalized difference between inverted and observed spectra is calculated. The iteration continues until this difference converges to a minimum value, which gives a better visual fit between observed and inverted displacement spectra that provides us the required model parameters, i.e., corner frequency, long-period spectral level and crustal Q values. Finally, using these model parameters, we calculate the other source parameters like source radius, static stress drop, seismic moment and moment magnitude, using empirical relations.

6.2 *Inversion procedure*

Taking the attenuation factor in to account the spectral amplitudes at a distance R from the source can be written as:

$$A(f, R) = \left(A_0/R^{-\lambda}\right) \exp\left(\pi R f/Q_0 V_s\right) \quad (1)$$

where A_0 is the amplitude at source, Q_0 is the dimensionless frequency independent S wave quality factor, f is the frequency, λ is the geometrical spreading and V_s is the S wave velocity. The frequency independent Q_0 is assumed in this analysis because it is the best fit for datasets (Boatwright *et al.* 1991; Atkinson and Mereu 1992; Fletcher 1995).

The exponential term can be written as:

$$\pi r f/Q_0 V_s = 1/2 * 2\,(\pi R f/Q_0 V_s) = \omega t^*/2 \quad \text{where } t^* = R/Q_0 V_s \tag{2}$$

where V_s is constant.

The equation (1) can be linearised by taking natural logarithm of both sides.

$$\ln A(f, R) = \ln A_0 - \lambda \ln R - \omega t^*/2. \tag{3}$$

At this point we assumed that λ equals to 1 to simplify the algebra (Fletcher 1995). Now following Boatwright (1980), A_0, the source term for S-waves (high frequency fall-off (γ) = 2) can be written as:

$$\begin{aligned} A_0 &= \Pi_0 / \left[1 + (f/f_c)^{2\gamma}\right]^{1/2} \\ &= \Pi_0 / \left[1 + (f/f_c)^4\right]^{0.5} \\ &= \left(\Pi_0 / B_4^{0.5}\right). \end{aligned} \tag{4}$$

Substitution of equation (4) into equation (3) yields:

$$\ln A(f, R) = \ln \Pi_0 \Big/ \left[1 + (f/f_c)^4\right]^{0.5} - \ln R - \omega t^*/2. \tag{5}$$

The B_4 term is expanded in a Taylor series as a Newton–Raphson's method for finding roots of non-linear equations (Press *et al.* 1992) and yields the final equation:

$$A(f) = \ln \Pi_0 - 0.5 \ln B_4 + 2B_4^{-1} (f/f_c)^4 (\Delta f_c/f_c) - \omega t^*/2. \tag{6}$$

'R' term is dropped because of the fact that the formula for moment is corrected from the geometrical spreading effect. Using least-squares algorithm with several iterations solves the model parameters.

The error is minimized in least squares sense by solving

$$\mathrm{D} = \mathrm{GM}. \tag{7}$$

The model parameter matrix M, sensitivity matrix G and data matrix D are

$$\mathrm{M} = \left[\ln \Pi_0,\, t^*,\, \Delta f_c\right]^T,$$

$$\mathrm{G} = \left[1,\, -\omega/2,\, 2\,\mathrm{B}_4^{-1} (f/f_c)^4 / f_c\right]$$

and

$$\mathrm{D} = [A(f) + 0.5 \ln \mathrm{B}_4] \tag{8}$$

Using Newton's method for quasi-linear equation

$$\Delta \mathrm{M} = \left(\mathrm{G}^{\mathrm{T}} \mathrm{G}\right)^{-1} \mathrm{G}^{\mathrm{T}} \Delta \mathrm{D} \tag{9}$$

where, ΔM is the change in model parameters and ΔD is the difference between predicted data and observed data. The solution is found iteratively $M_k = M_0 + \Delta M_{k-1}$ where M_0 is the initial model. Because the sensitivity matrix is near to singular here. We used Marquart–Lavenberg inversion technique to estimate the ln Π_0, t^* and Δf_c with 10 iterations. In the Marquart–Lavenberg inversion technique, it can be written as:

$$\Delta \mathrm{M} = \left(\mathrm{G}^{\mathrm{T}} \mathrm{G} + \lambda \mathrm{I}\right)^{-1} \mathrm{G}^{\mathrm{T}} \Delta \mathrm{D} \tag{10}$$

where ΔD is the difference between the predicted and observed data, λ is Levenberg–Marquardt adjustable damping parameter and I is the identity matrix. The Levenberg–Marquardt method is selected because (i) it combines beneficial aspects of Gauss–Newton and gradient methods while avoiding some of their weaknesses, (ii) the solution converges quickly, and (iii) in many cases a standard guess works well. In this study, λ value varies from 1 to 500.

The inversion begins with the initial guessed value of the model parameter (M_0); that is, corner frequency f_c, t^* and seismic moment M_0. The initial guessed value of f_c was set at 0.1 Hz for all events, while that of M_0 was selected visually from the respective low-frequency spectral level. And, the initial guessed value of t^* is calculated using the equation (2) (i.e., t^*=R/Q_oV_s, where R is the epicentral distance (in km). And for the Kachchh region, Q_o considers to be 102 while Vs assumes to be 3.5 km/s). At each iteration, the normalized difference between the computed spectra obtained from the theoretical formula and that yielded from equation (5) was computed. The maximum and minimum expected values of such difference were preset at the start of the iteration. The maximum difference was selected from the initial guessed values of M_0, t^* and f_c, and the minimum value was set based on the accuracy of the M_0, t^* and f_c values that one can expect to obtain from the inversion of noisy data. We also assign an initial value to λ, say 0.001. By substituting these initial guessed values into equation (10), the change in model parameter vector, ΔM, is derived. In the next iterations, a new model parameter is computed according to $M_{r+1} = M_r + \Delta M_r$, where M_r and ΔM_r are the model parameters and change in parameter values at the rth iteration.

7. Estimation of source parameters

After obtaining model parameters from the above-mentioned inversion technique source parameters like moment, source radius and stress drop are estimated using some empirical equations. These equations are:

$$\text{Seismic Moment } (M_0) = 4\pi\rho V_s^3 \mathrm{R}\rho\Pi_0/\mathrm{PFR}_{\theta\phi} \quad \text{(Brune 1970)} \tag{11}$$

$$\text{Source Radius } (r) = (2.34 * V_s) / (2\pi f_c) \quad \text{(Brune 1970)} \tag{12}$$

$$\text{Stress Drop } (\Delta\sigma) = (7/16) * \left(M_0/r^{**3}\right) \quad \text{(Keilis-Borok 1959)} \tag{13}$$

where 'V_s' and 'ρ' are the S wave velocity in m/s and rock density in gm/cm^3 at the source, respectively. Here, we calculate 'ρ' in kg /m^3 from $Vp = [(0.32V_p + 0.77)]$, where V_p is P-wave velocity in km/s] (Berteusen 1977). R denotes the hypocentral distance of the station in meters. 'R' is appearing in equation (11) to account for geometrical spreading term (1/R) in predicting ground motion for dominance of body waves for $R \leq 100$ km ($\approx$ roughly twice the crustal thickness) (Hermann 1985). A 'P' factor of $(1/\sqrt{2})$ accounting for the partitioning of energy in the two horizontal components and a free surface amplification factor (F) of 2 are used to estimate M_0. And the radiation factor ($\mathrm{R}_{\theta\phi}$) is considered to be 0.55 for the Kachchh region (Mandal and Johnston 2006), where deformation mode is mainly dominated by reverse faulting. The estimated 'M_0', 'r' and '$\Delta\sigma$' are in 'N-m', 'm', and 'MPa', respectively. And, the moment magnitude is estimated using the equation given below:

$$M_w = (2/3)\log_{10}(M_0) - 6.06 \quad \text{(Hanks and Kanamori 1979)} \tag{14}$$

where M_0 is in N-m.

Estimated hypocentral and source parameters for each event are listed in tables 2 and 3.

8. Error analysis

Here, we analyze the error in source parameters by estimating the standard deviation and mean of moment (M_0), source radius (r) and stress drop ($\Delta\sigma$). We also calculate the standard deviation for corner frequency (f_c) and frequency independent quality factor Q_0. The average seismic moment and source radius are estimated by the equations given below (Archuleta *et al.* 1982):

$$\langle M_0\rangle = \text{antilog}\left[(1/\mathrm{NS})\,\Sigma \log M_{0\mathrm{i}}\right] \tag{15}$$

and

$$\langle r\rangle = (1/\mathrm{NS})\,\Sigma\, r_{\mathrm{i}}. \tag{16}$$

The standard deviation of the log moment are calculated using the equation mentioned below:

$$\text{s.d. } (\log\langle M_0\rangle) = \left\{(1/\mathrm{NS}-1)\,\Sigma\left[\log M_{0\mathrm{i}} - \log\langle M_{0\mathrm{i}}\rangle\right]^2\right\}^{0.5}. \tag{17}$$

We also estimate multiplicative error factor using equation as given below:

$$E_{\mathrm{mo}} = \text{antilog}\left\{\text{s.d } (\log\langle M_0\rangle)\right\}. \tag{18}$$

Similarly, we calculate the average and the standard deviation for source radius, corner frequency and quality factor.

Finally, the standard deviations of stress drops are estimated using the equation as given below (Fletcher 1995):

$$\sigma_{\mathrm{std}} = \Delta\sigma\{((\sigma_{\mathrm{m}}/M_0)^2 + 9\,(\sigma_{\mathrm{r}}/r)^2\}^{0.5}. \tag{19}$$

From the above discussion, the standard deviation of moment, corner frequency, source radius, stress drop and quality factor and factor E_{mo} have been estimated for the selected 136 Bhuj aftershocks, which are recorded on three or more stations. The maximum standard deviation in corner frequency, stress drop and source radius are 0.73 Hz, 2.20 MPa, and 0.02 km, respectively (table 3). The mean values of standard deviation in corner frequency, stress drop, source radius and quality factor (Q) are 0.22 Hz, 0.19 MPa, 7 m and 4.26, respectively (table 3). For the standard deviation of 0.73 Hz in corner frequency leads to the standard deviation of 0.073 MPa in stress drop (table 3).

9. Results and discussions

We present the earthquake source parameters and crustal Q values, which have been estimated simultaneously using the Levenberg–Marquardt inversion of S-wave spectra of 144 selected aftershocks (2001–2010) of the 2001 M_w 7.7 Bhuj mainshock. The estimated static seismic moment (M_0), corner frequency (f_c), source radius (r) and static stress drop ($\Delta\sigma$) estimated from the inversion modelling of S-wave spectra of 144 aftershocks of magnitude 2.1 to 5.1 are ranging from 1.12×10^{12} to 4.00×10^{16} N-m, 2.36 to 8.76 Hz, 132.6 to 513.2 m and 0.01 to 20.0 MPa, respectively (table 3). The

Table 3. *Estimated source parameters and crustal Q values for selected 144 Bhuj aftershocks.*

Ev. nos	f_c(Hz)	s.d. $\langle f_c \rangle$	r (m)	s.d. $\langle r \rangle$	M_0(N-m)	s.d. $\langle M_0 \rangle$	$\Delta\sigma$ (MPa)	s.d. $\langle \Delta\sigma \rangle$	$E_{\rm mo}$	Q_0
1	2.68	0.32	492.00	62.0	2.33×10^{15}	0.26	1.05	0.4000	0.26	608.0
2	2.42	0.14	540.00	29.0	2.70×10^{15}	0.15	1.00	0.3500	0.18	435.0
3	2.80	0.09	467.00	14.0	5.10×10^{15}	0.20	2.20	0.5000	0.27	450.0
4	3.44	0.56	388.00	63.0	1.24×10^{14}	0.13	0.09	0.0300	0.10	923.0
5	2.36	0.15	388.00	63.0	8.30×10^{15}	0.17	2.20	0.3000	0.14	278.0
6	2.63	0.16	497.00	30.0	2.50×10^{14}	0.23	0.08	0.0300	0.19	510.0
7	2.54	0.00	513.00	0.0	1.80×10^{16}	0.27	5.70	0.0000	0.24	530.0
8	2.62	0.14	498.00	27.0	6.37×10^{16}	0.21	22.0	8.5000	0.40	893.0
9	7.49	0.04	185.98	0.91	2.16×10^{13}	0.04	0.15	0.0021	1.08	1108.6
10	5.38	0.40	252.00	0.22	8.00×10^{13}	0.22	0.22	0.0020	1.09	393.4
11	7.59	0.32	183.00	7.81	1.01×10^{13}	0.06	0.07	0.0094	1.16	1127.1
12	8.01	0.04	172.14	0.77	1.88×10^{12}	0.01	0.02	0.0002	1.02	429.9
13	7.09	0.14	227.40	4.32	5.85×10^{13}	0.26	0.24	0.0136	1.82	1138.1
14	7.48	0.30	178.00	7.19	1.27×10^{13}	0.15	0.10	0.0121	1.42	849.6
15	7.08	0.25	188.02	6.65	5.46×10^{13}	0.03	0.37	0.0394	1.07	1077.0
16	6.41	0.45	214.65	4.00	1.38×10^{14}	0.49	0.92	0.0515	3.10	418.2
17	7.70	0.09	165.85	1.97	5.41×10^{12}	0.24	0.06	0.0020	1.72	919.8
18	7.71	0.11	178.39	7.03	1.51×10^{13}	0.28	0.13	0.0158	1.90	825.5
19	7.81	0.27	176.44	6.11	6.77×10^{12}	0.18	0.06	0.0059	1.51	1263.5
20	7.73	0.19	178.43	4.37	9.46×10^{12}	0.24	0.08	0.0061	1.75	1092.1
21	7.71	0.39	179.00	7.89	2.31×10^{12}	0.09	0.02	0.0023	1.22	1000.5
22	8.04	0.37	171.56	7.89	2.03×10^{12}	0.00	0.02	0.0024	1.01	453.6
23	7.19	0.14	191.75	3.70	2.60×10^{13}	0.39	0.20	0.0116	2.43	1284.8
24	7.70	0.41	179.84	8.59	2.21×10^{12}	0.25	0.02	0.0025	1.78	1018.4
25	7.80	0.00	176.69	0.00	6.91×10^{12}	0.00	0.05	0.0000	0.00	988.2
26	7.48	0.44	184.55	11.26	1.23×10^{13}	0.14	0.09	0.0158	1.39	555.3
27	7.42	0.32	172.37	7.43	5.18×10^{12}	0.21	0.12	0.0160	1.62	493.0
28	7.31	0.23	188.68	5.84	4.44×10^{12}	0.04	0.03	0.0002	1.09	640.6
29	7.88	0.25	174.92	5.52	6.45×10^{12}	0.07	0.05	0.0051	1.18	947.2
30	7.76	0.27	177.74	6.11	2.53×10^{12}	0.30	0.02	0.0022	1.98	992.6
31	7.73	0.00	178.16	0.00	3.24×10^{12}	0.00	0.03	0.0000	0.00	701.9
32	7.64	0.14	174.02	3.23	3.51×10^{12}	0.23	0.03	0.0018	1.68	703.4
33	7.35	0.16	204.18	4.41	6.52×10^{12}	0.11	0.03	0.0022	1.27	1030.4
34	7.58	0.38	181.79	9.05	3.56×10^{12}	0.24	0.03	0.0047	1.73	491.4
35	7.65	0.22	180.35	5.08	5.39×10^{12}	0.13	0.04	0.0034	1.36	884.1
36	7.48	0.43	184.56	10.85	1.36×10^{13}	0.19	0.10	0.0173	1.54	869.0
37	8.19	0.23	168.25	4.75	2.81×10^{12}	0.03	0.03	0.0022	1.07	786.4
38	7.46	0.07	184.69	1.68	8.90×10^{12}	0.21	0.07	0.0018	1.63	874.1
39	7.37	0.32	187.27	8.32	8.43×10^{12}	0.09	0.06	0.0075	1.24	942.6
40	7.61	0.73	182.12	16.76	5.53×10^{12}	0.16	0.04	0.0120	1.45	1123.0
41	7.31	0.15	174.75	3.71	4.14×10^{12}	0.23	0.04	0.0023	1.71	668.9
42	7.15	0.52	193.47	13.56	5.05×10^{13}	0.29	0.33	0.0694	1.94	1068.3
43	7.18	0.51	192.71	14.34	4.10×10^{13}	0.37	0.29	0.0649	2.33	1215.8
44	7.65	0.21	180.25	4.79	1.16×10^{13}	0.09	0.09	0.0070	1.24	992.5
45	7.97	0.25	172.89	6.84	4.00×10^{12}	0.56	0.05	0.0060	3.40	1023.5
46	7.90	0.21	161.77	4.42	5.28×10^{12}	0.23	0.05	0.0044	1.69	826.2
47	7.73	0.00	171.97	0.00	1.46×10^{12}	0.00	0.03	0.0000	0.00	935.0
48	7.29	0.24	182.56	5.99	1.62×10^{13}	0.14	0.12	0.0058	1.39	1517.7
49	7.45	0.62	179.17	15.03	1.09×10^{13}	0.07	0.08	0.0211	1.17	751.4
50	7.73	0.37	178.48	8.35	4.05×10^{12}	0.12	0.03	0.0045	1.32	1038.2
51	7.61	0.04	181.18	0.85	5.36×10^{12}	0.34	0.05	0.0006	2.17	926.5
52	7.47	0.23	184.57	5.59	6.85×10^{12}	0.15	0.05	0.0047	1.42	842.5
53	8.13	0.39	169.69	8.31	2.96×10^{12}	0.19	0.03	0.0040	1.55	1019.3
54	7.22	0.30	191.20	8.01	8.21×10^{12}	0.17	0.05	0.0066	1.48	761.9
55	7.49	0.06	183.99	1.44	1.24×10^{13}	0.04	0.09	0.0021	1.09	876.9

Table 3. *(Continued)*

Ev. nos	f_c(Hz)	s.d. $\langle f_c \rangle$	r (m)	s.d. $\langle r \rangle$	M_0(N-m)	s.d. $\langle M_0 \rangle$	$\Delta\sigma$ (MPa)	s.d. $\langle \Delta\sigma \rangle$	$E_{\rm mo}$	Q_0
56	7.77	0.48	177.60	10.99	3.94×10^{12}	0.02	0.03	0.0057	1.06	495.9
57	8.07	0.20	170.89	4.20	3.61×10^{12}	0.24	0.04	0.0028	1.75	712.4
58	7.55	0.09	182.62	2.16	1.39×10^{13}	0.27	0.11	0.0039	1.86	951.1
59	6.51	0.11	211.80	3.44	6.76×10^{13}	0.18	0.32	0.0157	1.52	779.1
60	7.38	0.36	173.44	8.28	2.61×10^{13}	0.09	0.22	0.0314	1.24	758.0
61	6.05	0.00	227.74	0.00	8.19×10^{13}	0.00	0.30	0.0000	0.00	255.7
62	6.63	0.36	192.94	10.47	1.02×10^{14}	0.17	0.64	0.1046	1.47	586.5
63	6.70	0.65	196.69	15.04	3.31×10^{13}	0.19	0.20	0.0453	1.56	464.8
64	7.30	0.25	181.54	7.14	1.56×10^{13}	0.03	0.11	0.0133	1.06	588.2
65	7.24	0.22	190.35	5.76	6.84×10^{13}	0.13	0.44	0.0400	1.35	893.2
66	7.57	0.08	182.06	1.84	2.08×10^{13}	0.22	0.16	0.0049	1.68	696.8
67	6.90	0.33	200.02	9.54	1.10×10^{14}	0.16	0.61	0.0878	1.43	1035.4
68	7.46	0.15	184.70	3.75	1.59×10^{13}	0.05	0.11	0.0067	1.13	524.2
69	7.37	0.00	186.92	0.00	6.67×10^{12}	0.00	0.04	0.0000	0.00	468.5
70	8.10	0.06	170.12	1.23	6.12×10^{12}	0.11	0.06	0.0012	1.28	799.0
71	7.55	0.04	182.54	1.04	2.02×10^{13}	0.03	0.15	0.0025	1.08	999.1
72	8.60	0.11	152.0	3.30	1.10×10^{13}	0.32	0.13	0.0166	1.08	604.3
73	7.55	0.10	182.47	2.38	1.30×10^{13}	0.27	0.11	0.0041	1.85	563.5
74	6.96	0.35	191.36	9.99	6.04×10^{13}	0.32	0.42	0.0661	2.08	771.9
75	7.74	0.22	178.22	4.92	3.84×10^{12}	0.26	0.03	0.0027	1.81	875.7
76	7.71	0.02	178.73	0.41	2.27×10^{13}	0.14	0.18	0.0012	1.37	789.1
77	7.58	0.09	181.70	2.23	6.43×10^{12}	0.09	0.05	0.0017	1.23	1137.7
78	7.53	0.17	176.73	3.94	1.42×10^{13}	0.20	0.12	0.0081	1.57	679.1
79	7.54	0.17	176.36	3.97	9.02×10^{12}	0.23	0.08	0.0054	1.68	855.2
80	7.19	0.39	209.16	11.42	1.90×10^{13}	0.33	0.10	0.0171	2.11	920.7
81	7.66	0.17	173.51	3.90	3.72×10^{12}	0.22	0.04	0.0024	1.64	914.3
82	7.22	0.45	184.75	11.93	8.45×10^{12}	0.20	0.06	0.0116	1.59	1031.3
83	7.33	0.26	188.20	6.73	8.37×10^{12}	0.45	0.07	0.0072	2.80	553.3
84	7.40	0.00	179.64	0.00	6.23×10^{12}	0.00	0.05	0.0000	0.00	509.2
85	6.83	0.31	201.91	9.38	1.03×10^{14}	0.16	0.58	0.0804	1.44	603.6
86	7.48	0.16	184.34	3.91	3.52×10^{12}	0.14	0.03	0.0016	1.39	694.5
87	7.76	0.53	171.68	11.81	5.50×10^{12}	0.03	0.05	0.0099	1.06	1087.2
88	8.13	0.00	169.60	0.00	2.22×10^{12}	0.00	0.02	0.0000	0.00	1160.2
89	7.55	0.00	182.47	0.00	6.44×10^{12}	0.00	0.05	0.0000	0.00	781.6
90	7.55	0.03	169.12	0.56	3.28×10^{12}	0.22	0.03	0.0003	1.64	970.3
91	7.89	0.34	174.91	7.60	2.48×10^{12}	0.18	0.02	0.0027	1.51	854.5
92	8.04	0.02	164.37	7.31	2.85×10^{12}	0.22	0.04	0.0046	1.65	754.0
93	7.32	0.36	188.38	9.22	7.84×10^{12}	0.20	0.05	0.0080	1.57	1253.3
94	8.04	0.00	165.38	0.00	3.15×10^{12}	0.00	0.03	0.0000	0.00	561.2
95	7.04	0.29	188.97	7.69	9.04×10^{13}	0.23	0.65	0.0793	1.69	1240.5
96	7.89	0.12	190.35	2.97	4.79×10^{12}	0.12	0.03	0.0014	1.33	747.7
97	7.33	0.41	181.79	10.17	6.61×10^{12}	0.18	0.05	0.0087	1.48	790.7
98	7.51	0.16	183.57	3.92	3.37×10^{12}	0.31	0.03	0.0018	2.03	863.7
99	6.81	0.22	202.54	6.44	6.31×10^{13}	0.51	0.56	0.0532	3.24	864.1
100	7.84	0.31	172.65	2.38	4.78×10^{12}	0.07	0.04	0.0016	1.16	1265.6
101	8.18	0.10	156.11	1.83	2.18×10^{12}	0.25	0.03	0.0009	1.79	1109.5
102	8.14	0.10	169.36	2.02	5.85×10^{12}	0.01	0.05	0.0018	1.03	791.2
103	7.73	0.33	178.39	7.44	5.51×10^{12}	0.41	0.05	0.0064	2.56	1029.4
104	7.52	0.10	183.30	2.43	1.11×10^{13}	0.18	0.08	0.0033	1.53	827.6
105	7.85	0.23	175.54	5.01	4.24×10^{12}	0.35	0.04	0.0036	2.23	978.6
106	6.57	0.28	205.99	12.99	1.69×10^{13}	0.33	0.11	0.0200	2.11	1250.8
107	8.01	0.07	172.51	9.91	8.28×10^{12}	0.14	0.08	0.0131	0.37	998.3
108	6.80	0.23	204.41	6.86	5.12×10^{13}	0.21	0.29	0.0296	1.64	766.1
109	6.33	0.32	228.63	11.36	9.99×10^{13}	0.22	0.40	0.0595	1.65	432.6

Table 3. *(Continued)*

Ev. nos	f_c(Hz)	s.d. $\langle f_c \rangle$	r (m)	s.d. $\langle r \rangle$	M_0(N-m)	s.d. $\langle M_0 \rangle$	$\Delta\sigma$ (MPa)	s.d. $\langle \Delta\sigma \rangle$	E_{mo}	Q_0
110	7.42	0.31	185.81	7.64	3.16×10^{12}	0.27	0.03	0.0031	1.87	549.8
111	7.78	0.30	177.25	7.05	1.92×10^{12}	0.18	0.02	0.0019	1.52	1113.4
112	7.87	0.12	175.10	2.65	1.12×10^{12}	0.09	0.01	0.0004	1.22	468.4
113	8.11	0.00	169.92	0.00	2.48×10^{12}	0.00	0.02	0.0000	0.00	273.3
114	7.99	0.56	172.84	12.02	8.25×10^{12}	0.04	0.07	0.0150	1.09	309.0
115	7.64	0.30	182.06	7.22	2.15×10^{13}	0.36	0.20	0.0237	2.28	583.0
116	8.16	0.63	184.57	14.30	5.29×10^{12}	0.02	0.04	0.0086	0.05	1479.7
117	7.05	0.52	209.53	17.53	2.22×10^{13}	0.14	0.11	0.0269	1.38	1389.3
118	8.25	0.44	167.22	8.83	1.48×10^{12}	0.16	0.02	0.0024	1.46	705.2
119	6.98	0.41	198.93	13.36	1.17×10^{14}	0.14	0.71	0.1428	1.37	1526.0
120	7.58	0.17	168.63	3.80	2.60×10^{12}	0.03	0.02	0.0016	1.08	1021.8
121	8.26	0.41	167.16	8.28	1.33×10^{12}	0.24	0.01	0.0021	1.74	766.0
122	8.11	0.01	169.94	0.21	2.34×10^{12}	0.32	0.03	0.0027	2.10	699.9
123	7.64	0.00	211.11	0.00	2.65×10^{12}	0.00	0.01	0.0000	0.00	946.8
124	8.07	0.35	170.90	7.52	2.45×10^{12}	0.01	0.02	0.0029	1.02	830.8
125	7.93	0.33	182.44	7.69	2.24×10^{12}	0.40	0.02	0.0025	2.51	1136.0
126	7.15	0.33	202.30	9.24	9.39×10^{12}	0.16	0.05	0.0074	1.46	1221.1
127	7.86	0.24	132.57	5.08	1.85×10^{12}	0.47	0.02	0.0023	2.94	608.3
128	7.96	0.36	175.69	9.82	3.98×10^{12}	0.00	0.03	0.0055	1.01	588.4
129	7.74	0.12	186.80	2.78	1.46×10^{13}	0.26	0.11	0.0039	1.81	896.6
130	6.97	0.17	196.85	0.92	1.05×10^{13}	0.37	0.08	0.0010	2.36	1107.4
131	7.33	0.18	197.18	4.73	8.96×10^{13}	0.31	0.60	0.0431	2.03	640.9
132	6.90	0.17	201.44	5.05	1.48×10^{14}	0.35	0.97	0.0725	2.22	710.0
133	8.76	0.00	183.95	0.00	4.23×10^{12}	0.00	0.03	0.0000	0.00	1881.9
134	7.58	0.18	180.01	4.10	9.47×10^{12}	0.42	0.11	0.0075	2.61	682.2
135	7.02	0.02	196.35	0.59	4.87×10^{12}	0.14	0.03	0.0002	1.39	885.6
136	7.74	0.20	180.37	4.69	9.95×10^{12}	0.09	0.07	0.0058	1.24	676.3
137	7.32	0.24	188.37	6.20	4.67×10^{12}	0.14	0.03	0.0031	1.38	1099.6
138	7.76	0.00	198.18	0.00	6.34×10^{12}	0.00	0.04	0.0000	0.00	504.9
139	7.58	0.00	181.86	0.00	2.61×10^{12}	0.00	0.02	0.0000	0.00	1152.3
140	8.60	0.17	152.00	4.87	1.00×10^{13}	0.13	0.13	0.0020	1.36	659.3
141	8.08	0.24	170.62	5.06	9.86×10^{12}	0.31	0.05	0.0046	2.02	816.6
142	7.99	0.00	159.87	0.00	2.77×10^{12}	0.00	0.03	0.0000	0.00	417.4
143	8.04	0.00	171.34	0.00	3.51×10^{12}	0.00	0.03	0.0000	0.00	356.7
144	8.22	0.00	167.59	0.00	3.27×10^{12}	0.00	0.03	0.0000	0.00	316.0

crustal S-wave 'Q' varies from 139 to 1880, with an average of 840 for the region (table 3).

Next, we present 23 S-wave spectra of 11 events with moment magnitude varying from 2.1 to 5.1, which are estimated at nine different stations, i.e., TAP, GDD, VJP, BHU, TPM, MTP, BHA, SKL and RPR. The date, time, magnitude and corner frequency of events, and adjustable damping parameter (λ) used for the Levenberg–Marquardt inversion of S-wave spectra are also shown in figures 3–5. For this study, the sampling rate of broadband data is 100/50 sps, thus the maximum frequency content of spectra is defined by the nyquist frequency (sps /2), i.e., 50/25 Hz. The TAP station (out of seven stations considered here) is situated on the hard Jurassic sediments, which is clearly reflected by the stable nature of S-wave spectra for earthquakes of $M_w > 2.5$ as seen from figures 3(a–h), 4(a–h), and 5(a–g). However, the spectra for smaller earthquakes of $M_w \leq 2.5$ at TAP station show some abrupt changes in spectral amplitude at 1–9 Hz (figures 4 and 5). From the S-wave spectra at all stations except TAP, an abrupt fluctuation in the spectra is noticeable at 0.2–3.0 Hz (figures 3–5), which could be associated with the site amplification caused by low velocity sediments at 0.2–3.0 Hz (Mandal *et al.* 2008). We also notice poor fitting of S-wave spectra between 20 and 25 Hz (figures 3–5), which could be due to large variation in attenuation factor (k) associated with the low velocity sediments in the Kachchh rift basin.

We plot the estimated corner frequencies with their error bars *versus* $\log_{10}(M_0)$ in figure 6(a). The calculated corner frequencies range from 2.36

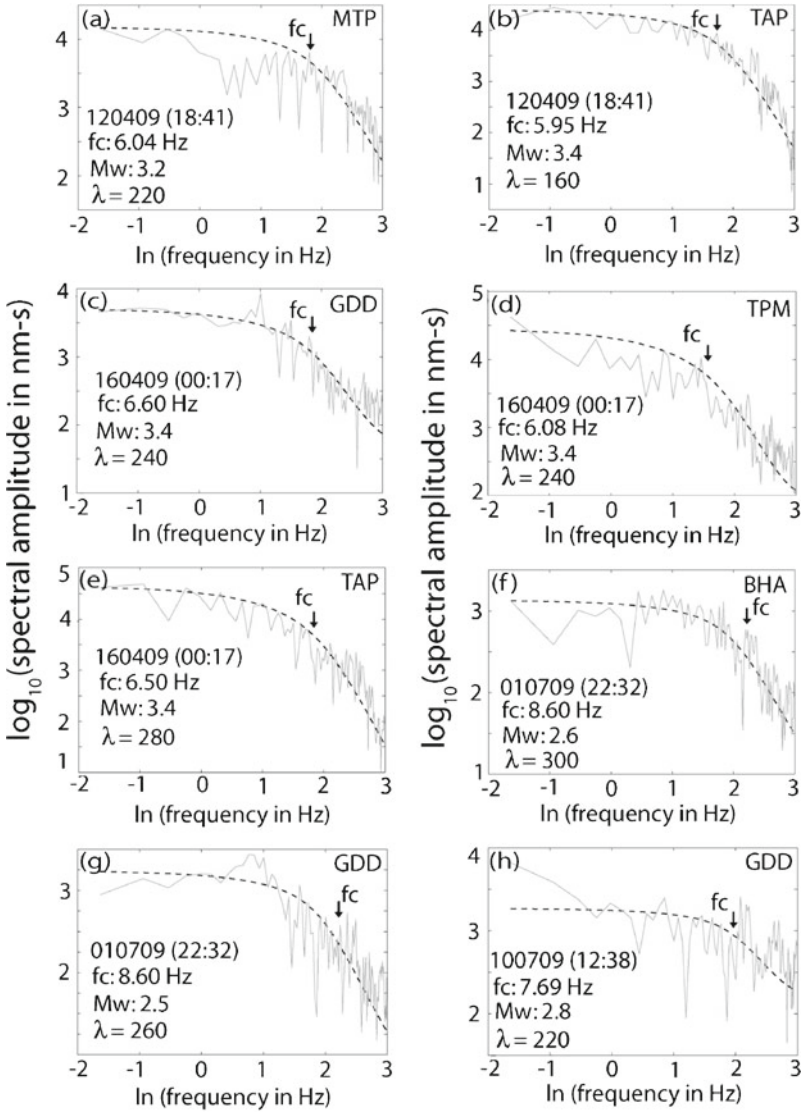

Figure 3. Cross plot of $\log_{10}$(spectral amplitude of S-wave (in nm-sec)) and ln(frequency (in Hz)). Estimated S-wave spectra (solid grey line) and modeled spectra from inversion (dotted grey line) for the Bhuj aftershocks at different broadband sites (**a**) for an M_w 3.2 event at MTP, (**b**) for an M_w 3.4 event at TAP, (**c**) for an M_w 3.4 event at GDD, (**d**) for an M_w 3.4 event at TPM, (**e**) for an M_w 3.4 event at TAP, (**f**) for an M_w 2.6 event at BHA, (**g**) for an M_w 2.5 event at GDD, and (**h**) for an M_w 2.8 event at GDD. The date of occurrence, origin time, moment magnitude, corner frequency and corresponding adjustable damping parameter (λ) used for Levenberg–Marquardt inversion of S-wave spectra for each event are shown. A black arrow showing the corresponding corner frequency (f_c) for each event is also shown.

to 8.76 Hz. The maximum standard deviation or error in corner frequency is estimated to be 0.73 Hz (figure 6a; table 3). What is also obvious from figure 6(a, b) is that the relation between corner frequency and seismic moment can be separated in two regions. For events seismic moment smaller than about $10^{14.2}$ N-m, the logarithmic regression of corner frequency and seismic moment has a slope of -0.043 while the slope is found to be -0.033 for larger seismic moment events ($>10^{14.2}$ N-m). Thus, this observation indicates that seismic moments of smaller earthquakes in the Kachchh region do exhibit a different source scaling than the larger events with seismic moment larger than $10^{14.2}$ N-m. The seismic moment of $10^{14.2}$ N-m corresponds to a moment magnitude 3.4. We also notice that the estimated corner frequencies are found to decrease with the increasing moment magnitude values as expected. The maximum standard deviation or error in corner frequency is estimated to be 0.73 Hz (table 3).

The estimated seismic moments are plotted against the source radius in log-log plot with the constant stress drop lines (figure 7a), which show that the source radii for smaller events ($M_0 \leq 10^{14.2}$ N-m) are weakly dependent on event size, compared with larger events ($M_0 > 10^{14.2}$ N-m) where source radii increase with increasing

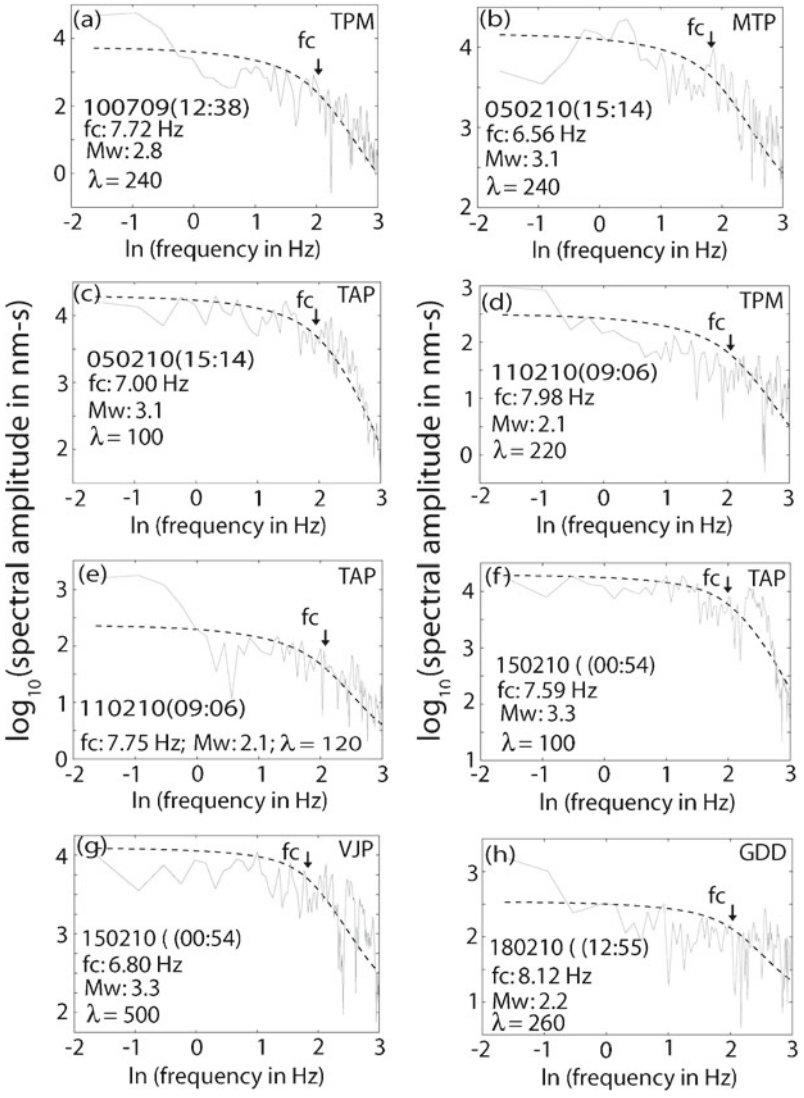

Figure 4. Same as figure 3. (**a**) For an M_w 2.8 event at TPM, (**b**) for an M_w 3.1 event at MTP, (**c**) for an M_w 3.1 event at TAP, (**d**) for an M_w 2.1 event at TPM, (**e**) for an M_w 2.1 event at TAP, (**f**) for an M_w 3.3 event at TAP, (**g**) for an M_w 3.3 event at VJP, and (**h**) for an M_w 2.2 event at GDD.

moment. This seems to suggest that a critical source radius may exist for intraplate earthquakes that would characterize the lower part of the magnitude range. Its value is around 200 m in source radius for the earthquakes in the Kachchh region we analyzed. The estimated error or standard deviations in source radii are found to be ranging from 0.20 to 19.34 m. For events seismic moment smaller than about $10^{14.2}$ N-m, the logarithmic regression of seismic moment and source radii has a slope of 9.28, which is larger than the expected slope for a constant stress drop, while the same slope is estimated to be 5.33 for larger events with seismic moment larger than $10^{14.2}$ N-m (figure 7b). Thus, this observation indicates that seismic moments of smaller earthquakes in the Kachchh region do not exhibit a constant stress drop.

In figure 8(a), we plot logarithm of static stress drops (in MPa) and logarithm of seismic moment (in N-m). The calculated stress drops are found to be varying from 0.01 to 20.0 MPa. The standard deviations of stress drops are found to be 0.0002 to 2.21 MPa (table 3). We notice that the relation of stress drop and seismic moment can be separated into two regions above and below about $10^{14.2}$ N-m in moment, like the source radius and corner frequency relation with seismic moment. The stress drops for events with the seismic moment less than about $10^{14.2}$ N-m increase with increasing moment, then become less dependent on moment for the larger events. The seismic moment of $10^{14.2}$ N-m corresponds to a moment magnitude 3.4. Our estimated stress drops reveal a more systematic nature ($\log_{10}\Delta\sigma = 0.88\ \log_{10}M_0 - 12.6$)

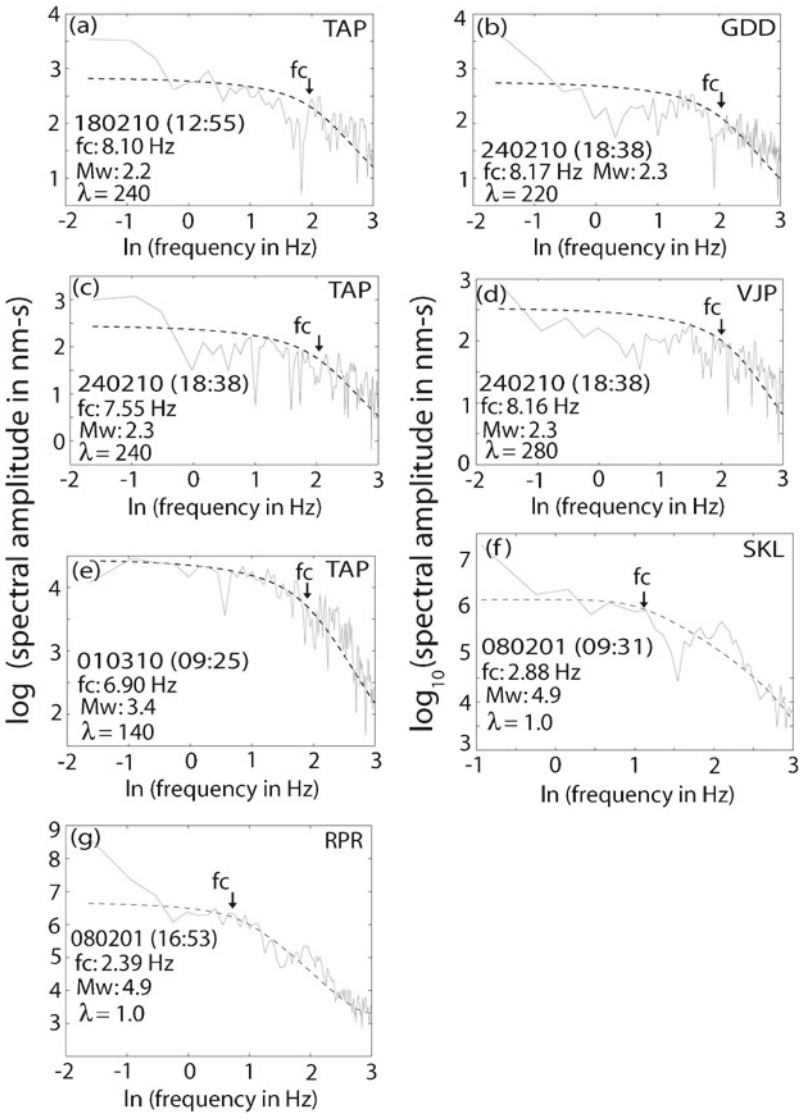

Figure 5. Same as figure 3. (**a**) For an M_w 2.2 event at TAP, (**b**) for an M_w 2.3 event at GDD, (**c**) for an M_w 2.3 event at TAP, (**d**) for an M_w 2.3 event at VJP, (**e**) for an M_w 3.4 event at TAP, (**f**) for an M_w 4.9 event at SKL, and (**g**) for an M_w 4.9 event at RPR.

for smaller moment values (log $M_0 \leq 10^{14.2}$ N-m, smaller aftershocks), while, in the region with seismic moment larger than $10^{14.2}$ N-m, estimated stress drop define a different relation ($\log_{10}\Delta\sigma = 0.19 \log_{10} M_0 - 12.6$) for moderate size aftershocks (figure 8a). However, Mandal and Johnston (2006), based on their source parameter study of 300 Bhuj aftershocks, suggest a systematic scaling ($M_0^3 \propto \Delta\sigma$) for smaller seismic moments, whereas they suggest more scatter value for large M_0 value, suggesting on an average a scaling ($M_0^n \propto \Delta\sigma$) where n varies from 0.5 to 1. Thus, we infer that our results are in good agreement with the findings of Mandal and Johnston (2006).

Figure 8(b) reveals that large stress drops are confined to the 15–30 km depth range, which perhaps indicates the existence of the base of seismogenic layer in the same depth range. The maximum stress drop value is estimated to be 20.0 MPa at 29.3 km depth for the largest studied event of M_w 5.1, which occurred in 2006 on the NWF fault in a reverse sense of motion. We also plot the stress drop of 21 MPa for the 2001 Bhuj mainshock, which is taken from Antolik and Dreger (2003). The observed large stress drops in the 15–30 km depth range could be attributed to crustal mafic intrusives and presence of aqueous fluids in the lower crust as revealed by the earlier tomographic study of the region. The spatial distribution of estimated stress drops is shown in figure 9, which suggests a concentration of larger stress drops (>2.2 MPa) on the south dipping reverse NWF, the causative fault of the 2001 Bhuj mainshock. The calculated stress drops for two events, which took place on the almost vertical strike-slip GF, suggest a low stress drop value of the order of 0.035 MPa (table 3).

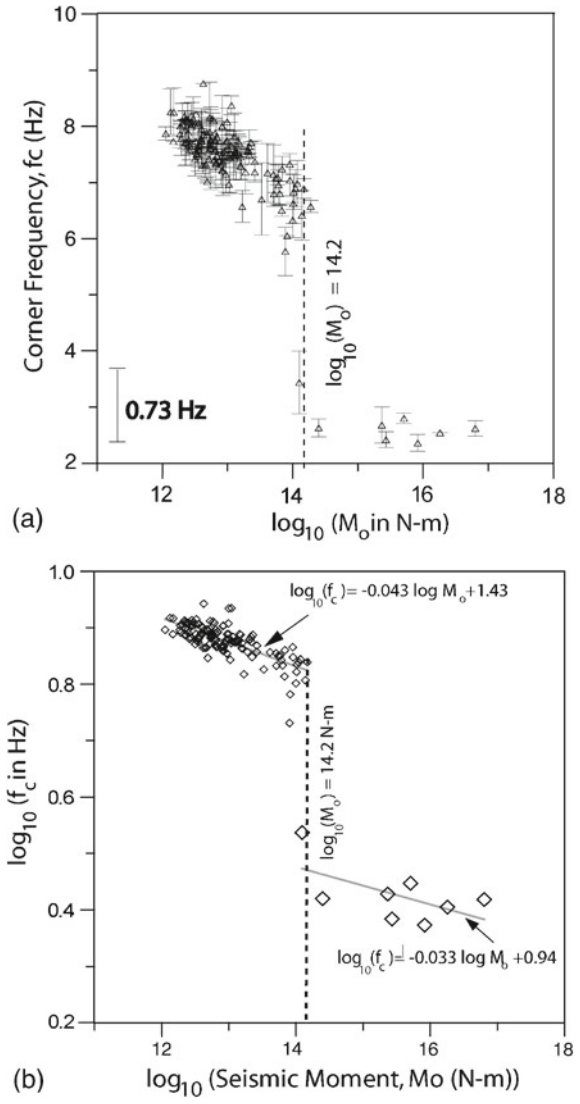

Figure 6. (**a**) Logarithmic plot between seismic moment, M_0 (in N-m) and source radii, r (in m). The 'M_0' and 'r' for the 1993 Latur, 1997 Jabalpur and the 2001 Bhuj earthquakes are shown by bigger black solid circles. (**b**) Cross plot between $\log_{10}(f_c$ in Hz) with error bars and $\log_{10}(M_0$ in N-m).

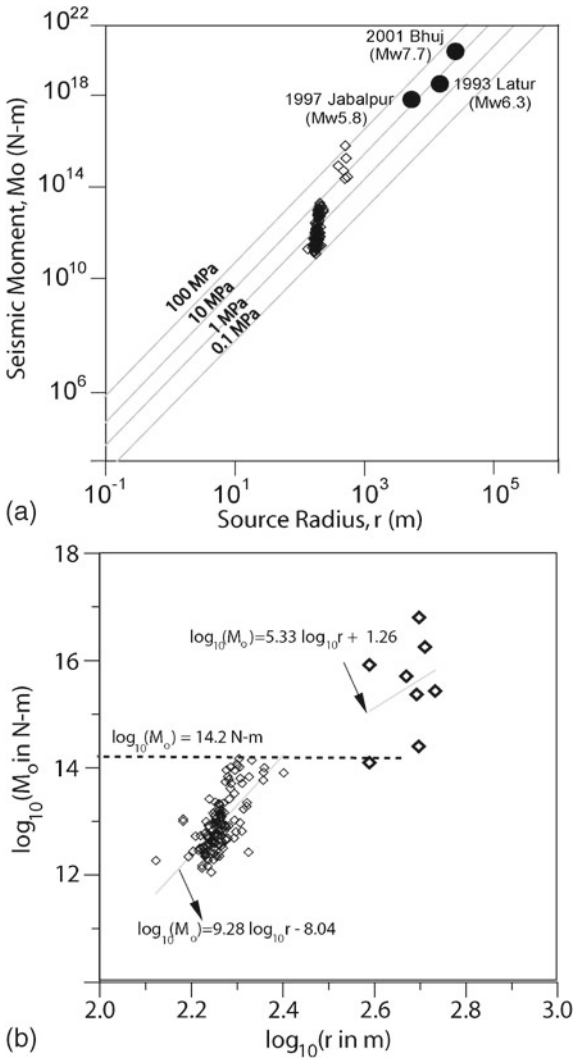

Figure 7. (**a**) Logarithmic plot between the seismic moment (M_0, in N-m) and stress drops ($\Delta\sigma$, in MPa). (**b**) Depth distribution of estimated stress drops of selected 144 aftershocks (marked by open squares). The stress drop estimate of the 2001 Bhuj mainshock (marked by large solid black circle) is taken from Antolik and Dreger (2003).

It is well known that uncertainty in Q estimates can lead to significant error in earthquake source parameter estimates. In the same connection, we discuss here all available frequency dependent Q-estimates for the Kachchh region. Singh *et al.* (2004) have estimated a relation $Q(f) = 800f^{0.42}$ for the Indian shield region using the dataset of four earthquakes recorded in the distance range of 240–2400 km. In 2004, Bodin *et al.* (2004) estimated a frequency dependent Q_0 (Q_c at 1 Hz) value of 790 for the Kachchh region from their study on ground motion modelling. Further, Mandal *et al.* (2004a, 2004b) found a frequency dependent Q_0 (Q_c at 1 Hz) value of 102 for the Kachchh region, based on their study on the coda-Q_c study. Recently, Sharma *et al.* (2008) have also obtained a frequency dependent Q_0 value of 148 based on coda-Q_c study. Now, we know that the coda-based method used in Mandal *et al.* (2004a, 2004b) and Sharma *et al.* (2008) gives the low Q of a very shallow portion of the crust, while large Q estimates obtained by Singh *et al.* (2004) and Bodin *et al.* (2004) sample deeper in the crust. Next, we discuss our estimates of frequency independent average crustral Q, which are ranging from 256 to 1882 with an average of 840 for the region. The large value of crustal Q thus obtained ($Q = 840$), indicates a low shear-wave attenuation for the near-surface rocks of the Kachchh region, which can also explain the observation of an intensity XI close to the epicenter and severe damage up to 350 km away from the

epicenter of the 2001 Bhuj mainshock. Further, our estimates for crustal average Q are agreeing well with the findings of Singh *et al.* (2004) and Bodin *et al.* (2004). We also observe that our average crustal Q-value of 840 is very similar to Q_0 (Q_c at 1 Hz) value (∼900) of the New-Madrid region, USA (Bodin *et al.* 2004). Thus, we can infer that the ground motion attention characteristics for the Kachchh and New Madrid regions are expected to be similar as observed by Bendick *et al.* (2001) in terms of similar variation in intensity with distances in these regions.

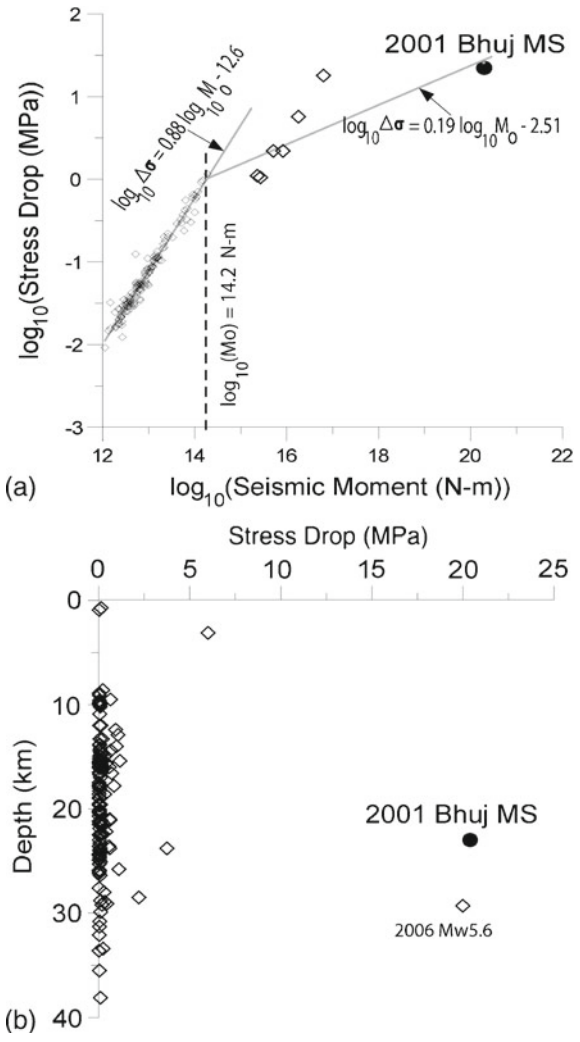

Figure 8. Spatial distribution of stress drops. The north Wagad fault and Gedi fault are marked by NWF and GF, respectively. Solid large black circle marks the stress drop (∼21 MPa) of the 2001 Bhuj mainshock while solid medium size grey circles mark the larger stress drop estimates (> 2.2 MPa) for three aftershocks of M_w 4.4–4.9, which have occurred during 2001–2006. Solid large grey circle marks the stress drop (∼20 MPa) of the 2006 M_w 5.1 event. The stress drop estimates for other selected aftershocks (2009–2010) are shown by open black circles (medium size for $1.0 < \Delta\sigma \leq 2.2$ MPa and smaller size for $\Delta\sigma \leq 1.0$ MPa).

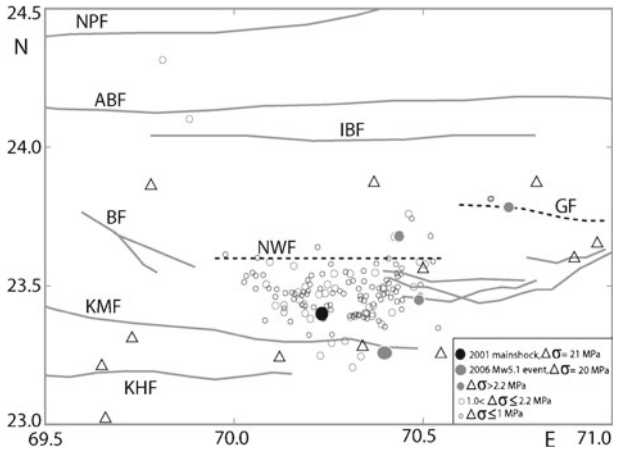

Figure 9. Spatial distribution of stress drops. The north Wagad fault and Gedi fault are shown by black dotted lines and marked as NWF and GF, respectively. Solid large black circle marks the stress drop (∼21 MPa) of the 2001 Bhuj mainshock while solid medium size grey circles mark the larger stress drop estimates (> 2.2 MPa) for three aftershocks of M_w 4.4–4.9, which have occurred during 2001–2006. Solid large grey circle marks the stress drop (∼20 MPa) of the 2006 M_w 5.1 event. The stress drop estimates for other selected aftershocks (2009–10) are shown by open black circles (medium size for $1.0 < \Delta\sigma \leq 2.2$ MPa and smaller size for ≤ 1.0 MPa).

Next we present a comparative study of stress drops between the 2001 Bhuj aftershocks and various other intraplate earthquakes in India. The estimated stress drops of the M_w 7.7 2001 Bhuj, 1993 M_w 6.3 Latur and 1997 M_w 5.8 Jabalpur earthquakes are reported to be 21, 7, and 20 MPa, respectively (Baumbach *et al.* 1994; Antolik and Dreger 2003; Singh *et al.* 2004), while the stress drops of the reservoir triggered Koyna earthquake sequence (1994–1997) range from 0.03 to 19 MPa for events with M_w varying from 1.5 to 4.7 (Mandal *et al.* 1998). Interestingly, we notice that our estimated stress drop of 20 MPa for an M_w 5.1 aftershock is larger than that of the 1993 M_w 6.3 Latur earthquake (∼7 MPa, Baumbach *et al.* 1994). This could be attributed to the rift tectonics of the Kachchh region, whereas, the Latur region is characterized by tectonics of stable continental regions. We know that Kachchh rift zone is characterized by a high velocity lower crust (Mandal and Pandey 2010), which can explain the estimated large stress drop of 20 MPa for an M_w 5.1 Bhuj aftershock at 29.3 km depth in the mafic lower crust. Similarly, Mandal and Dutta (2011) also notice larger stress drop of 6.17 MPa (for an M_w 4.7 Bhuj aftershock) at 7 km below the NWF. Thus, it is apparent that the stress drops are found to be relatively less in the intermediate crust (6–14 km), but they reach their maximum in the lower crust (14–34 km depth).

This kind of depth dependency of stress drop values can be attributed to the increase in maficness of crustal rocks with increasing crustal depth below the main rupture zone of the 2001 Bhuj earthquake (Mandal and Pandey 2010).

10. Conclusions

The Fletcher's (1995) simultaneous inversion method provides an improved constraint on the estimation of source parameters of aftershocks of the 2001 M_w 7.7 Bhuj earthquake and crustal S-wave Q for the region. The estimated source parameters are robust and appearing to be more realistic than those obtained from the routine S-wave spectral analysis of Bhuj aftershocks.

The simultaneous estimation of source parameters and crustal Q for 144 selected Bhuj aftershocks of moment magnitude 2.1 to 5.1 led to following significant findings:

- The estimated seismic moment, stress drop, corner frequency, source radius and crustal Q are ranging from 1.12×10^{12} to 4.00×10^{16} N-m, 0.01 to 20 MPa, 2.36 to 8.76 Hz, 132.6 to 513.2 km and 256 to 1882, respectively.
- The estimated source radii for smaller events ($M_0 \leq 10^{14.2}$ N-m) are weakly dependent on event size, compared with two larger events ($M_0 > 10^{14.2}$ N-m).
- For aftershocks of the 2001 Bhuj intraplate earthquake we analyzed, a critical source radius of around 200 m characterizes the lower part of the magnitude range.
- Interestingly, corner frequency, source radii and stress drop estimates show a distinctly different behaviour for smaller (seismic moment $\leq 10^{14.2}$ N-m) and larger (seismic moment $>10^{14.2}$ N-m) aftershocks for the 2001 Bhuj earthquake.
- Most interestingly, the estimated stress drop values for Bhuj aftershocks show more scatter ($\log_{10}\Delta\sigma = 0.19\ \log_{10}M_0 - 12.6$) towards the larger seismic moment values ($>10^{14.2}$ N-m, larger aftershocks), whereas, they show a more systematic nature ($\log_{10}\Delta\sigma = 0.88\ \log_{10}M_0 - 12.6$) for smaller seismic moment ($\leq 10^{14.2}$ N-m, smaller aftershocks) values.
- This inversion technique would be very efficient for estimating earthquake source parameters for any virgin area of unknown crustal Q values.
- Estimated S-wave Q values are found to be ranging from 139 to 1880 with an average of 840 for the Kachchh region, which is very similar to Q_0 value ($\sim$900) of New Madrid region, USA.
- The estimated large stress drops in the 15–30 km depth range are attributed to the presence of crustal intrusive and aqueous fluids in the lower crust below the main rupture zone of the 2001 M_w 7.7 Bhuj earthquake.

Acknowledgements

Authors are thankful to the Director, NGRI for his encouragement and kind permission to publish this work. This study was supported by the Ministry of Earth Sciences, New Delhi.

References

Antolik M and Dreger D S 2003 Rupture process of the 26 January 2001 M_w 7.6 Bhuj, India, earthquake from teleseismic broadband data; *Bull. Seismol. Soc. Am.* **93** 1235–1248.

Archuleta R J, Cranswick E, Muellar C and Spudich P 1982 Source parameters of the 1980 Mammoth Lakes, California, Earthquake sequence; *J. Geophys. Res.* **87** 4595–4607.

Atkinson G and Mereu R 1992 The shape of ground motion attenuation curves in southeastern Canada; *Bull. Seismol. Soc. Am.* **82** 2014–2031.

Baumbach M, Grosser H, Schmidt H G, Paulat A, Rietbrock A, Rao C V R K, Soloman Raju P, Sarkar D and Mohan I 1994 Study of the foreshocks and aftershocks of the intraplate Latur earthquake of September 30, 1993, India; *Geol. Soc. India Memoir* **35** 33–63.

Bendick R, Bilham R, Fielding E, Gaur V K, Hough S E, Kier G, Kulkarni M N, Martin S, Mueller K and Mukul M 2001 The 26 January 2001 'Republic Day' earthquake, India; *Seismol. Res. Lett.* **72** 328–335.

Berteusen K A 1977 Moho depth determinations based on spectral ratio analysis of NORSAR long-period P waves; *Phys. Earth Planet Interior* **31** 313–326.

Biswas S K 1987 Regional framework, structure and evolution of the western marginal basins of India; *Tectonophys.* **135** 302–327.

Boatwright J 1980 A spectral theory for circular seismic sources: Simple estimates of source dimension, dynamic stress drop and radiated energy; *Bull. Seismol. Soc. Am.* **70** 1–27.

Boatwright J, Fletcher J B and Fumal T E 1991 A general inversion scheme for source, site, and propagation characteristics using multiply recorded sets of moderate-size earthquakes; *Bull. Seismol. Soc. Am.* **81** 1754–1782.

Bodin P and Horton S 2004 Source parameters and tectonic implications of aftershocks of the M_w 7.6 Bhuj earthquake of 26 January 2001; *Bull. Seismol. Soc. Am.* **94** 818–827.

Bodin P, Malagnini L and Akinci A 2004 Ground motion scaling in the Kachchh Basin, India, deduced from aftershocks of the 2001 M_w 7.6 Bhuj earthquake; *Bull. Seismol. Soc. Am.* **94** 1658–1669.

Brune J N 1970 Tectonic stress and the spectra of seismic shear waves from earthquakes; *J. Geophys. Res.* **75** 4997–5009.

Bureau of Indian Standards (BIS) 2002 Criteria for Earthquake Resistant Design of Structures (Fifth Revision), 39p.

Chung W Y and Gao H 1995 Source parameters of the Anjar earthquake of July 21, 1956, India and its seismo-tectonic implication for the Kutch rift basin; *Tectonophys.* **242** 281–292.

Dodge D A, Beroza G C and Ellsworth W L 1996 Detailed observations of California foreshock sequences: Implications for the earthquake initiation process; *J. Geophys. Res.* **101** 22,371–22,392.

Fletcher J B, Boatwright J, Linda H, Hanks T and Macgarr A 1984 Source parameters for aftershocks of the Oroville, California, earthquake; *Bull. Seismol. Soc. Am.* **74** 1101–1123.

Fletcher J B 1995 Source parameters and crustal Q for four earthquakes in South Carolina; *Seismol. Res. Lett.* **66** 44–58.

Gupta H K, Harinarayana T, Kousalya M, Mishra D C, Mohan I, Rao P N, Raju P S, Rastogi B K, Reddy P R and Sarkar D 2001 Bhuj earthquake of 26 January 2001; *J. Geol. Soc. India* **57** 275–278.

Hanks T C and Kanamori H 1979 A moment magnitude scale; *J. Geophys. Res.* **84(B5)** 2348–2350.

Havskov J and Ottemoller L 2003 SEISAN: The Earthquake Analysis Software, manual.

Johnston A C 1994 Seismotectonic interpretation and conclusions from the stable continent regions; In: *The earthquakes of stable continental regions: Assessment of large earthquake potential*; Electric Power and Research Institute, Palo Alto, Report TR 10261.

Johnston A C and Schweig E S 1996 The enigma of the New Madrid earthquake of 1811–1812; *Ann. Rev. Earth Planet.* **24** 339–384.

Keilis-Borok V K 1959 An estimation of the displacement in earthquake source and of source dimensions; *Ann. Geofis.* **12** 205–214.

Kumar M R, Saul J, Sarkar D, Kind R and Shukla A K 2001 Crustal structure of the Indian shield: New constraints from teleseismic receiver functions; *Geophys. Res. Lett.* **28** 1339–1342.

Lee W H K and Valdes C M 1985 HYP071PC: A personal computer version of the HYPO71 earthquake location program; U.S. Geological Survey, pp. 85–749.

Mandal P, Rastogi B K and Sarma C S P 1998 Source parameters of Koyna Earthquakes, India; *Bull. Seismol. Soc. Am.* **88(3)** 833–842.

Mandal P, Rastogi B K, Satyanarayana H V S, Kousalya M, Vijayraghavan R, Satyamurthy C, Raju I P, Sarma A N S and Kumar N 2004 Characterization of the causative fault system for the 2001 Bhuj earthquake of M_w 7.7; *Tectonophys.* **378** 105–121.

Mandal P, Srivastava J, Joshi S, Kumar S, Bhunia R and Rastogi B K 2004 Low coda-Q_c in the epicentral region of the 2001 Bhuj Earthquake of M_w 7.7; *Pure Appl. Geophys.* **161** 1635–1654.

Mandal P 2006 Sedimentary and crustal structure beneath Kachchh and Saurashtra regions, Gujarat, India; *Physics of the Earth and Planetary Interiors* **155** 286–299.

Mandal P 2007 Sediment thickness and Q_s *vs.* Q_p relations in the Kachchh rift basin, Gujarat, India using Sp converted phases; *Pure Appl. Geophys.* **164** 135–160.

Mandal P 2011 Crustal and lithospheric thinning beneath the seismogenic Kachchh rift zone, Gujarat (India): Its implications towards the generation of the 2001 Bhuj earthquake sequence; *J. Asian Earth Sci.* **40** 150–161.

Mandal P and Johnston A 2006 Estimation of source parameters for the aftershocks of the 2001 M_w 7.7 Bhuj earthquake, India; *Pure Appl. Geophys.* **163** 1537–1560.

Mandal P and Horton S 2007 Relocation of aftershocks, focal mechanisms and stress inversion: Implications towards the seismo-tectonics of the causative fault zone of M_w 7.6 2001 Bhuj earthquake (India); *Tectnophys.* **429** 61–78.

Mandal P and Pandey O P 2010 Relocation of aftershocks of the 2001 Bhuj earthquake: A new insight into seismotectonics of the Kachchh seismic zone, Gujarat, India; *J. Geodyn.* **49** 254–260.

Mandal P and Dutta U 2011 Estimation of earthquake source parameters and site response; *Bull. Seismol. Soc. Am.* **101(4)** 1719–1731.

Mandal P, Dutta U and Chadha R K 2008 Estimation of site response in the Kachchh seismic zone, Gujarat, India; *Bull. Seismol. Soc. Am.* **98(5)** 2559–2566.

Mandal P, Satyamurthy C and Raju I P 2009 Iterative deconvolution of the local waveforms: Characterization of the seismic sources in Kachchh, India; *Tectonophys.* **478** 143–157.

McCaplin J P and Thakkar M G 2001 Bhuj-Kachchh earthquake: Surface faulting and its relation with neotectonics and regional structure, Gujarat, Western India; *Ann. Geophys.* **46** 937–956.

Negishi H, Mori J, Singh R P and Kumar S 2001 Aftershocks and slip distribution of mainshock: A comprehensive survey of the 26 January 2001 Bhuj earthquake (M_w 7.7) in the state of Gujarat, India; Research Report on Natural Disaster, pp. 33–35.

Press *et al.* 1992 Numerical Recipes in Fortran and C; Academic Press, 382p.

Rastogi B K, Gupta H K, Mandal P, Satyanarayana H V S, Kousalya M, Raghavan R, Jain R, Sarma A N S, Kumar N and Satyamurty C 2001 The deadliest stable continental region earthquake occurred near Bhuj on 26 January 2001; *J. Seismol.* **5** 609–615.

Rajendran C P and Rajendran K 2001 Character of deformation and past seimicity associated with 1819 Kachchh earthquake, northwestern India; *Bull. Seismol. Soc. Am.* **91(3)** 407–426.

Reddy P R, Sarkar D, Sain K and Mooney W D 2001 Report on collaborative scientific study at USGS, Menlo Park, USA (30 October–31 December, 2001), 19p.

Sharma B, Gupta A K, Devi K D, Kumar D, Teotia S S and Rastogi B K 2008 Attenuation of high-frequency seismic waves in Kachchh Region, Gujarat, India: *Bull. Seismol. Soc. Am.* **98(5)** 2325–2340.

Singh S K, Pacheco J F, Bansal B K, Perez-Campos X, Dattatrayam R S and Suresh G 2004 A source study of the Bhuj, India Earthquake of 26 January, 2001 (M_w 7.6); *Bull. Seismol. Soc. Am.* **94(4)** 1195–1206.

Wesnousky S G, Seeber L, Rockwell T K, Thakur V, Briggs R, Kumar S and Ragona D 2001 Eight days in Bhuj: Field report bearing on surface rupture and genesis of the 26 January, 2001 earthquake in India; *Seismol. Res. Lett.* **72(5)** 514–524.

Williams R L F 1958 The Black Hills – Kutch in history and legend, Weidenfeld and Nicolson, London.

MS received 13 October 2011; revised 30 March 2012; accepted 9 September 2012